Title: Calcium: Modulator of Post-transcriptional and post-translational process in mESCs

Shikha Sharma, Dasaradhi Palakodeti, Tina Mukherjee

Short title: Calcium and mESCs pluripotency

Author List

Dr Shikha Sharma: First author, lead contact and corresponding author

Affiliation: Institute for Stem Cell Science and Regenerative Medicine (inStem), Bangalore, India, 560065

E-mail: shikha.ss19254@gmail.com

Orcid ID: https://orcid.org/ 0000-0002-0364-3162

Dr Dasaradhi Palakodeti

Affiliation: Institute for Stem Cell Science and Regenerative Medicine (inStem), Bangalore, India, 560065

E-mail: dasaradhip@instem.res.in

Dr Tina Mukherjee

Affiliation: Institute for Stem Cell Science and Regenerative Medicine (inStem), Bangalore, India, 560065

E-mail: tinam@instem.res.in

Abstract

Calcium ion (Ca^{2+}) is a ubiquitous intracellular and extracellular messenger that regulates several cellular activities. Previous findings have reported the presence of active Ca^{2+} receptors in mouse embryonic stem cells (mESCs) but the fundamental requirement of Ca^{2+} signalling remains unclear. We have noted the presence of high Ca^{2+} in undifferentiated mESCs and showed that its depletion exerts G2/M cell cycle arrest, spontaneous differentiation of mESCs towards mesoderm lineage and mitochondrial biogenesis. Further, our data demonstrates that Ca^{2+} regulates the homeostasis and stability of Oct4 and Nanog at the post-translational level through pCamkIIα dependent mechanism independent of polyubiquitin system, JAK-STAT3 pathway, transcriptional and translational control. Our data also signifies the role of Ca^{2+} at the post-transcriptional level in regulating p-bodies and stress granule markers (Dcp1a, XRN1, Tudor and EDC4), splicing-dependent and 3'UTR-dependent NMD activity. Together, this study identifies the broad role of Ca^{2+} in modulating key processes in mESCs.

Keywords: Calcium; p-bodies; cell-cycle arrest; pluripotency; mitochondrial biogenesis

Highlights

- Ca^{2+} is present at elevated levels in mESCs and is important for pluripotency
- Ca^{2+} depletion accelerates G2/M cell cycle arrest and mesoderm differentiation
- Ca^{2+} regulates pluripotency and p-bodies markers at the post-translational level
- Ca^{2+} regulates Oct4, Nanog, dcp1a through pCaMKIIα dependent mechanism

Introduction

Embryonic stem cells (ESCs) are derived from the inner cell mass (ICM) of embryos defined by eminent features such as pluripotency, self-renewal, and limitless proliferation (Ye et al., 2024). Several studies have shown that the ESCs' core pluripotency network is regulated by diverse molecular mechanisms, extracellular signalling pathways, post-transcriptional regulation, epigenetic mechanisms, and chromatin remodelling (Yeo and Ng, 2013, Kobayashi and Kikyo, 2015). The ability of ESCs to differentiate into all three lineages of an organism makes them an ideal candidate for basic research on pluripotency, genomic engineering, cell identity transition, disease modelling, cell therapy, and regenerative medicine (Kobayashi and Kikyo, 2015, Czechanski et al., 2014). Further understanding the regulation of ESCs' pluripotency network will provide more insight into the nature of pluripotent stem cells, cell fate decision, and lineage specification.

Ca^{2+} is a fundamental regulator of several processes such as cell cycle, cell proliferation, neuronal plasticity, gene regulation, and apoptosis (Clapham, 2007, Berridge et al., 2003). Despite the broad role of Ca^{2+} signalling in different cell types, there are only a few studies that have reported the presence of Ca^{2+} signalling in pluripotent stem cells. In 2004, Yanagida et al. documented the activation of various Ca^{2+} receptors upon stimulation in mESCs, indicating the presence of calcium-regulating pathways (Yanagida et al., 2004). Todorova et al. (2009) observed the activation of Ca^{2+} signalling by lysophosphatidic acid (LPA) in mESCs. In 2010, Schwirtlich et al. reported that GABA-mediated Ca^{2+} signalling is important for the proliferation and differentiation of mESCs. Recently, it was demonstrated that high intracellular calcium is paramount for regulating naïve pluripotent state and self-renewal of mESCs, suggesting the importance of calcium in controlling the pluripotency of

mESCs (Zhu and Zhang, 2019, MacDougall et al., 2019). However, the role of Ca^{2+} signalling in the regulation of pluripotency remains unclear. In this study, we have reported the role of Ca^{2+} signalling in regulating proliferation, cell cycle, p-bodies dynamic and core pluripotency markers of mESCs. Our data indicates that high Ca^{2+} is important for the maintenance of pluripotency in mESCs at the post-transcriptional and post-translational levels.

Results

Pluripotent stem cells maintain an elevated level of cytosolic calcium

Using fluo4 staining, we observed a high level of Ca^{2+} in undifferentiated mESCs compared to spontaneously differentiated mESCs cultured in the absence of LIF (Fig. 1A and 1D). It is not yet clear why undifferentiated mESCs maintain a high level of Ca^{2+} within their cytoplasm. Therefore, we became interested in understanding the role of Ca^{2+} in mESCs. We manipulated the level of Ca^{2+} in the presence of LIF using BAPTA-AM (Bapta) and thapsigargin. Bapta is a highly selective cell-permeable Ca^{2+} chelator (Collatz et al., 1997), and thapsigargin is a SERCA pump inhibitor known to increase intracellular Ca^{2+} in various cell types including ESCs (Lytton et al., 1991, Huang et al., 2017). We observed using Fluo-4 staining that supplementation of Bapta 2uM (B2uM) for 72hours was able to reduce the level of Ca^{2+} in mESCs, comparable to without LIF condition (C-L), while thapsigargin 1nM (T1nM) treatment increased the calcium level (Fig. 1A and 1D). We also noted that Ca^{2+} was downregulated in the C-L condition, and supplementation of T1nM in C-L condition was able to increase the Ca^{2+} level slightly but was unable to bring it back to the control condition (C+L) (Fig. 1A and 1D). We also detected heterogeneity in the level of Ca^{2+} in cells within mESCs colonies (Fig. 1A). In addition, we noted that B1uM also reduced the Ca^{2+} level in

the different organelles, such as endoplasmic reticulum (ER) (Fig. 1B and 1E) and lysosomes (Fig. 1C) of mESCs. Conversely, T1nM increased the overall Ca^{2+} level in the lysosomes (Fig. 1C) but not in the ER (Fig. 1B and 1E).

Further, we have observed a decrease in the proliferation of mESCs with the increase in the concentration of bapta (B1uM, B2uM, and B5uM) in 72 hrs (Fig. 1F). We noted that mESCs colonies exhibited fibroblast morphology upon differentiation and observed increased differentiation with increasing concentrations of bapta (B1uM and B2uM) (Supplementary file S1 (S1)_Supplementary Fig. S2C and S2D). Indeed, we also observed that differentiation was less in bapta-treated samples compared to C-L, but they exhibited fibroblast morphology similar to C-L condition (S1_ Supplementary Fig. S2C and S2D). We further replaced B2uM media after 72 hours with control ESC media (B2R) for 48 hours and observed an increase in the proliferation of mESCs, indicating bapta treatment is reversible (Fig. 1G). However, we noted that mESCs that underwent complete morphological change (fibroblast appearance) were unable to proliferate further and had retained their phenotype. Several studies have revealed that cMyc is important for maintaining the unlimited proliferation of mESCs, and its depletion exerts dormancy and proliferation arrest (Scognamiglio et al., 2016; Fagnocchi et al., 2016; Ruan et al., 2017). We next checked the level of cMyc within these mESCs and observed that cMyc expression goes down upon B2uM treatment in 72 hours, independent of transcriptional control (Fig. 1H and 1K), which indicated that Ca^{2+} might be regulating proliferation in mESCs by controlling cMyc expression. We further observed an increase in the expression of cMyc in B2R compared to B2uM in 5 days (Fig. 1I and 1J). Besides this, we analysed the cell cycle profile of C+L, B2uM, and B2R mESCs in 72 hrs (Fig. 1L) and 5 days (Fig. M), and observed that B2uM treatment resulted in the cell cycle arrest at G2/M,

which was reversible with B2R treatment (Fig. M). Earlier reports in mesenchymal stem cells (MSCs) and epidermal stem cells suggested that high calcium is crucial for stem cell proliferation and cell cycle progression; and G2 phase of cell cycle is important for the determination of Ca^{2+} signalling pattern (Moore et al., 2024, Vallet et al., 2025) . Further, we also noted that B2uM and C-L resulted in the fluctuation in the expression of calcium receptors of the plasma membrane, ER and mitochondria including SERCA PMCA, IP3, STIM, ORAI, Ryanodine, and MCU (S1_Supplementary Fig. S1C, D, E, F, G, H), which signifies that bapta treatment might be affecting the level of Ca^{2+} within different organelles.

Calcium homeostasis is critical for pluripotency

To explore the role of Ca^{2+} in the maintenance of pluripotency in mESCs, we checked the expression of pluripotency markers upon bapta and thapsigargin treatment. Western blot and immunofluorescence (IF) data confirmed the increase/decrease in the protein level of core pluripotency markers including Oct4 and Nanog upon low/high Ca2+ condition using bapta (B1uM and B2uM) and thapsigargin 250 pM, 500pM and 1nM (T250pM, T500pM, T1nM) in the presence of LIF, suggesting that Ca^{2+} has role in the regulation of pluripotency markers (Fig. 2 A, B, E, F and M). Moreover, we noted the heterogeneity in the expression of Oct4 and Nanog in cells within mESCs colonies (Fig. 2A and 2B), which also corroborates with the heterogeneous level of Ca^{2+} in cells within mESCs (Fig. 1A). Next, we have not observed any significant difference in the expression of Oct4, Nanog, and cMyc in the absence of LIF and the presence of thapsigargin (Fig. 2 A, B, G, H, and M). CHIR 99021 (CH) and PD0325901 (PD) are inhibitors of glycogen synthase kinase 3 beta (GSK3β) and MAPK/ERK signalling pathways, also known as 2i inhibitors implicated for the maintenance of the ground state of mESCs (Sim et al., 2017). Furthermore, we subjected mESCs to 2i

inhibitor treatment in the presence of LIF and B1uM and observed a decrease in the expression of Oct4 and Nanog (S1_Supplementary Fig. S2A), which signifies that Ca^{2+} regulates the expression of pluripotency markers under naive and ground state of mESCs. We also discerned that some of the mESCs colonies exhibited fibroblast morphology upon B1uM treatment in the presence of a 2i inhibitor (S1_Supplementary Fig. 2B).

Phosphorylated CaMKIIα (pCaMKIIα) is an eminent downstream target of Ca^{2+} signalling (Clapham 2007). When intracellular calcium level increases, calcium interact with calmodulin and activates CaMKIIα by phosphorylating it at T286, which induces autonomous activation of CaMKIIα making it sustain pCaMKIIα level for some time, when calcium level drops (Clapham 2007, Chi et al., 2016). We checked the expression of pCaMKIIα using the pCaMKIIα (Thr 286) monoclonal antibody. Our data showed Ca^{2+}-dependent simultaneous upregulation/downregulation of pCaMKIIα and Oct4 in mESCs upon B2uM and T1nM treatment for 72 hours (Fig. 2B, 2C, and 2M). We further noted that pCaMKIIα is present mainly in the nucleus of mESCs and observed the co-localization of pCaMKIIα with Oct4 (Fig. 2E, yellow), indicating that Ca^{2+} might have a role in the regulation of phosphorylation of pluripotency markers through a pCaMKIIα-dependent mechanism. Previous reports suggest that LIF plays a major role in maintaining the pluripotency of mESCs mainly through the JAK-STAT3 pathway (Tang and Tian, 2013, Ohtsuka et al., 2015). We asked if Ca^{2+} regulates the LIF signalling by controlling the JAK-STAT pathway in mESCs. We observed that the protein level of pSTAT3 was unchanged upon B1uM, B2uM, T250pM, T500pM, and T1nM treatment in the presence and absence of LIF, suggesting that Ca^{2+} might not be playing role through JAK-STAT3 pathway for the maintenance of pluripotency of mESCs (Fig. 2 E, F, and H). Further, we checked the

transcript level of Oct4, Nanog, Sox2 and Klf4, and early differentiation markers of mesoderm (Mixl1, Brachyury), endoderm (Sox17, and MeoX1), and ectoderm (Sox1, and Pax6) upon Ca^{2+} manipulation using B2uM and T1nM and observed no change in the transcript level of these markers in 48hrs (S1_Sipplementary Fig. 1A and 1B) and 4 days (Fig. 2I and 2J). Therefore, our data indicate that Ca^{2+} might be playing a role in the regulation of pluripotency and differentiation markers at the post-transcriptional, translational, and post-translational levels.

Besides this, we observed an increase in the cytoplasm-to-nucleus ratio of mESCs by decreasing the level of Ca^{2+} using B2uM and C-L conditions, and a decrease in the cytoplasm-to-nucleus ratio upon T1nM treatment by phalloidin staining, shown by the arrow (Fig. 2K and 2L). Park et al. have also demonstrated that high cytosolic Ca^{2+} results in a decreased cytoplasm/nuclear ratio in drosophila C4da neurons (Park et al., 2020), which also corroborates with our findings and indicates the possible role of Ca^{2+} in cytoskeleton remodelling for cell shape transition. Cadherin-adhesion complex is important for bridging cell-to-cell contact and drives various morphogenetic changes (Mege and Ishiyama, 2017). Therefore, we checked the expression of calcium-dependent adhesion protein E-cadherin and found its expression downregulated in mESCs upon B2uM treatment and increased upon T1nM condition, indicating the involvement of Ca^{2+}-dependent cadherin family proteins for driving morphological changes in ESCs upon Ca^{2+} manipulation (Fig. 2N).

Calcium is important for the regulation of ribonucleoprotein complexes and NMD activity

To understand whether Ca^{2+} has any role at the post-transcriptional level. We examined the expression of p-bodies and stress granule markers upon Ca^{2+} manipulation in mESCs. Our data showed that dcp1a, xrn1, Tudor and b-actin are present abundantly in both cytoplasm and nucleus of undifferentiated mESCs (Fig. 3A and 3B, S1_Supplementary Fig. S3A, B, C, and D) and observed a decrease/increase in the expression of these mRNP granules upon B2uM and T1nM treatment (Fig. 3A, B, D, S1_Supplementary Fig S3 A, B, C, D, E). We also noted the variation in the size of these granules, as some were large in size and others small (Fig. 3B). The variations in size could be due to several reasons, such as a) these markers may be a part of several complexes having different compositions, either present as a monomer or dimer b) they may be at different stages of maturation for post-transcriptional processes to carry out their functions. Further, we have observed the co-localization of dcp1a with b-actin, xrn1, tudor, and pCaMKIIα, indicating that Ca^{2+} might be regulating p-body markers through a pCaMKIIα-dependent mechanism (Fig. 3B). However, we were unable to check the co-localization of other markers with pCaMKIIα as both the antibodies were raised in the same species. Our data also shows that Ca^{2+} regulates p-bodies and stress granule markers independent of transcriptional control (Fig. 3C). Next, we have quantified splicing-dependent nonsense-mediated mRNA decay (NMD) activity and long 3' UTR-dependent NMD activity in B2uM and C-L conditions using two fluorescent reporter proteins, green TagGFP2 and far-red Katushka, as described by Pereverzev et al. 2015. We have observed increased splicing-dependent NMD activity (Fig. 3E and 3F) and decreased 3' UTR NMD activity (Fig. 3G and 3H) in mESCs treated with B2uM and C-L conditions, suggesting that Ca^{2+} exerts the opposite effect on splicing-dependent and 3'UTR-dependent NMD pathways in mESCs. As we have not observed any change in the transcript level of pluripotency and differentiation markers. This also raises a possibility that p-bodies, stress granule markers, and NMD in mESCs might be playing a major role in the regulation of markers other than

pluripotency and differentiation markers, and further studies are needed to identify those markers.

Calcium doesn't control the expression of pluripotency and differentiation markers at the post-transcriptional and translational level

We checked the global translation rate through polysome profiling and observed no change in the global translational rate upon Ca^{2+} manipulation with B2uM in 72 hours (Fig. 4A). However, we observed that the expression of early translation initiation marker elf1a was downregulated in B2uM-treated mESCs in 72 hours (Fig. 4B). which indicates a possibility of differential expression of translation markers upon Ca^{2+} manipulation. We have observed no change in the transcription of pluripotency and differentiation markers in control and B2uM-treated mESCs (S1_Sipplementary Fig. 1A and 1B, Fig. 2I and 2J). We sought to find whether Ca^{2+} suppresses the translation of pluripotency/differentiation markers by holding them in p-bodies/stress granules. To address this, we performed polysome profiling of mESCs treated with B2uM for 72 hours and collected cytoplasmic fraction (composed of mRNP granules), 80s ribosomal subunit (80s), and polysome fraction, and checked the expression of Oct4, Nanog, Sox2, and Klf4 and early differentiation markers of mesoderm, and ectoderm, such as Mixl1, Brachyury, Pax6 exhibiting high CT value. We were unable to detect any significant difference in the transcript level of both pluripotency and differentiation markers in the cytoplasmic fraction of mRNP granules, the 80S and polysome fraction of control and B2uM-treated samples (Fig. 4D and 4E), indicating that pluripotency and differentiation markers are not held by p-bodies and might also not be regulated at the translational level. As we observed no change in the transcript level of core pluripotency and early differentiation markers, To affirm this further, we blocked the transcription and

translation of control, B1uM, T1nM and C-L treated mESCs after 72hrs with combined actinomycin D (ACD) cycloheximide (CHX) treatment for 2hr and checked the expression of pluripotency and mesodermal differentiation markers and observed no significant change in their expression, which illustrate that Ca^{2+} doesn't regulate core pluripotency and differentiation markers at transcriptional and post-transcriptional level (Fig. 4F and 4G).

It is known that undifferentiated ESCs either do not express or express low levels of differentiation markers (Ghimire et al., 2018). We noted that the transcript level of early differentiation markers such as MixL1 and Brachyury was expressed at CT values of 28±1 and 28±1, respectively, while MeoX1 expressed a CT value of 28±1, and SOX17 was mostly undetermined or expressed at a CT value of 34±1, Pax6 and SOX1 were present at CT values of 26±1 and 26±1 respectively in undifferentiated mESCs. These CT values signify that transcripts of differentiation markers are present at a low level in undifferentiated mESCs. In addition, we detected transcript of differentiation markers (MixL1, Brachyury, and Pax6) in a polysome fraction of control and B2uM treated mESCs (Fig. 4D and 4E), which indicates that differentiation markers are undergoing translation and might be expressed in undifferentiated mESCs or getting degraded. Since these mESCs showed a tendency to spontaneous differentiation towards mesoderm lineage (fibroblast morphology). We have checked the expression of only brachyury protein in control, B2uM and C-L condition (Fig. 4H). We have observed some background expression of brachyury in undifferentiated mESCs and its increased expression in B2uM and C-L conditions (Fig. 4H), which indicates the role of calcium in the degradation of brachyury protein in C+L condition. Next, we also performed mitotracker-red staining and noted the increase in the size and number of mitochondria upon calcium reduction with B2uM and C-L condition in 48hrs (Fig. 4I, and

4J), we observed globular mitochondria in control mESCs and a network of branched mitochondria in B2uM and C-L in 48hrs (Fig. 4I), indicating mitochondria undergo a morphological change from globular to tubular form upon Ca^{2+} reduction.

Calcium is important for the stability of pluripotency markers, p-body and stress granule markers, and degradation of differentiation markers

Further, we asked whether Ca^{2+} plays a role in the degradation of proliferation, differentiation, core pluripotency markers, polyubiquitin marker (pUBQ), p-body, and stress granule markers at post-translational level. Our data demonstrate an increase in the expression of cMyc, dcp1a, tudor, Oct4, and pUBQ in both control and B2uM-treated mESCs upon MG132 treatment (Fig. 5 A, B, C, D, E, F, G), which suggests that Ca^{2+} level might be important for the maintenance of homeostasis and stability of these proteins. Further, we also observed increased expression of brachyury in the control condition after MG2132 treatment, which also corroborates with the increased expression of brachyury upon B2uM treatment but MG132 was unable to increase the brachyury protein expression in B2uM treated mESCs but rather it led to its decreased expression (Fig. 5A and 5D). Earlier findings have suggested that proteasomal inhibition can lead to the degradation of proteins through the activation of other degradation pathways such as autophagy (Wang et al., 2019). Furthermore, we noted that MG132 treatment was able to rescue only partial protein levels of dcp1a and tudor in B2uM-treated mESCs compared to control mESCs (Fig. 5B and 5F), which also implies the role of other signalling pathways in the regulation of p-body and stress granule markers upon Ca^{2+} reduction. Interestingly, we also noted the decrease in the expression of pUBQ upon B2uM treatment and its upregulation with MG132 treatment (Fig. 5C and 5D), which suggests that Ca^{2+} might be regulating the stability of pluripotency markers independent of PUBQ

proteasomal system upon Ca^{2+} reduction. Next, we observed a very low expression of LC3 in the undifferentiated mESCs, which further decreased upon B2uM and C-L condition, suggesting autophagy might not be playing a role in the degradation of pluripotency and differentiation markers upon Ca^{2+} reduction (Fig. 5H). Our study also indicates that the pUBQ proteasomal system might be important for the degradation of differentiation markers in undifferentiated mESCs, and its low expression upon Ca^{2+} reduction is important for the stability of brachyury protein and activation of other signalling pathways apart from autophagy to determine lineage specificity. We have further checked the stability of Oct4 and Nanog using a CHX chase assay as described by Kao et al., 2015. We chased the expression of Oct4 and Nanog for 1hr 20 min with a 20 min time interval and observed that their degradation was faster in B2uM-treated mESCs, indicating that Ca^{2+} is important for the maintenance of the stability of core pluripotency markers (Fig. 5I). Furthermore, we observed an increase in the level of Oct4 and Nanog proteins in B2uM-treated mESCs with MG132 treatment (Fig. 5J), suggesting that Ca^{2+} maintains the stability of pluripotency markers at the post-translational level.

Calcium maintains the stability of OCT4, NANOG, and DCP1a by a pCaMKII alpha-dependent mechanism

In order to affirm the role of calcium signalling in the regulation of pluripotency and p-body markers, we performed the knockdown the pCaMKIIα, the main downstream target of calcium signalling to estimate the decreased calcium level effect and serca-R2 knockdown to observe increase calcium effect on calcium signalling. We used the electroporation method to deliver the CaMKIIα shRNA to silence the pCaMKIIα protein expression. The CaMKIIα shRNA targets and silence the CaMKIIα mRNA and prevents the production of

unphosphorylated and active pCaMKIIα protein (Moore et al., 2010, Hirst et al., 2022). We noted that 80-90% of mESCs expressed CaMKIIα shRNA as shown by their GFP expression (Fig. 6A). Moreover, we observed that CaMKIIα shRNA treated mESCs exhibited fibroblast-like morphology (Fig. 6B and 6C), which was similar to the phenotype shown by B2uM treated mESCs (Fig. 2K). However, we were unable to detect any significant decrease in the level of CaMKIIα mRNA but observed a decrease in the level of pCaMKIIα protein (pCaMKIIα KD) upon CaMKIIα shRNA treatment (Fig. 6D and 6I), which suggests the possibility that CaMKIIα shRNA might have exerted an indirect mechanism in regulating pCaMKIIα protein expression rather than canonical knockdown efficiency, and this might be through stress granules, translational control, or protein instability, or a decrease in RNA pool was not detected by qPCR. Furthermore, we detected a significant decrease in the expression of Oct4 and Nanog proteins upon pCaMKIIα KD by western blotting (Fig. 6F); however, we did not observe any change in the transcript level of both pluripotency and differentiation markers (Fig. 6M and 6N), similar to B2uM-treated mESCs (Figure 2I and 2J). In addition, we observed that the pSTAT3 protein level was unaffected in pCaMKIIα KD mESCs, which again signifies that Ca^{2+} might not be playing role through JAK-STAT pathway (Fig. 6F). We further observed a decrease in the expression of p-body marker dcp1a upon pCaMKIIα KD (Fig. 6I), which indicates that Ca^{2+} is important for the stability of dcp1a through a pCaMKIIα-dependent mechanism. Furthermore, we also performed SERCA-R2 receptor knockdown (SER-R2 KD) by using shRNA against its highly expressed receptor2, which we have noted in our QPCR data. We observed a decrease in the mRNA pool of the SERCA-R2 receptor upon SER-R2 KD (Fig. 6D). We noted that SER-R2 KD mESCs exhibited compact colonies as compared to control mESCs (Fig. 6B and 6C), which was similar to T1nM-treated mESCs (Fig. 2K). Furthermore, we observed an increase in the expression of Oct4 and Nanog proteins upon SER-R2 KD (Fig. 6G). We observed no change

in the transcript level of pluripotency and differentiation marker (Fig. 6M and 6N) as well as in the protein level of pSTAT3 in SER-R2 KD mESCs (Fig. 6G), again signifying that calcium might not be acting through JAK-STAT pathway. Furthermore, we also observed an increase in the expression of dcp1a and pCaMKIIα upon SER-R2 KD (Fig. 6H), which indicates that cytosolic Ca^{2+} plays a role in the biogenesis of dcp1a through pCaMKIIα.

Identification of phosphoproteins altered upon calcium manipulation using a phosphoproteomics approach

We explored the pooled phosphoproteomics profile of control and B2uM-treated mESCs. We identified 53 phosphoproteins (PP) that were significantly upregulated and 35 PP downregulated in B2uM samples (n=2 each set pooled phosphoproteomic) shown by the heat map (Fig.7A and Supplementary file S2 (S2)_Supplementary Table 1, 2, 3, 5). Using Proteome Discoverer Software (Thermo Fisher Scientific), we detected the phosphosites in the identified phosphopeptides from mass spectrometry (MS) data and observed majorly serine-threonine phosphosites along with a few tyrosine sites, which (S2_Supplementary Table 1 and 4), which indicate that Ca^{2+} manipulation through bapta majorly influence broad category of serine-threonine PP. Further using ShinyGO 0.80 software, we carried out the KEGG pathway, tree plot, GO cellular component (GOC), and string function enrichment analysis for the differentially expressed phospho-proteins (DEPP) represented in the heat map (Fig. 7B, C, D, E, F). We observed that spliceosome and mRNA surveillance PP were highly enriched in our dataset and carried out further KEGG pathway enrichment analysis for them (Fig. 7G and 7H) and observed that our PP are part of these complexes labelled as red. We further observed that DEPP exhibits 1385 protein-protein interactions (PPI) with an expected 689 PPI (p=0) using string PPI network analysis (Fig. 7I). Next, we identified DEPP related

to different pathways using string bio process enrichment analysis (SBPEA). We conducted GO biological function (GOB), GO molecular function (GOF) and GOC analysis for DEPP related to metabolism listed in the legend of Supplementary Fig. 4 A, and observed that they are the positive and negative regulator of metabolism, part of mRNP complex and displayed nuclear and organelle localization which suggests a widespread functional role of these proteins (S1_Supplementary Fig. S4A, 4B, 4C). Further, we carried out the GOC analysis of a few DEPP, including Hk2, Hspa8, Atp5a1, Cox4i1, Pkm, and Gapdh, identified for ATP metabolism, and observed they have mitochondrial localization (S1_Supplementary Fig. S4J), which signifies their role in mitochondrial biogenesis and oxidative phosphorylation. We also noted that several PP related to translational machinery including Rps18, Rp16, Eif3c, Abcf1, Eef1a1, Eef2, Eif5a, Rpl18a, Eif2s1, Rpl5, Rplp2, Rpl34, Eef1d, Rpl27, Eif3b, Rpl23a, Rps8, and Larp1 were highly differentially regulated (Fig. 7A), despite global translation rate was unaffected upon Ca^{2+} reduction and conducted GOC, GOB network and GOF analysis for them (S1_Supplementary Fig. S4G, 4H and 4I). We observed that these proteins are also part of the mRNP complex and have a role in macromolecule biosynthetic pathway, which exemplify their other role apart from controlling translation rate. Next, we further performed the GOB and GOF analysis for DEPP implicated in nucleosome and chromatin assembly, including Smarcd1, Nasp, Hat1, Atrx, and Nap1l1 (S1_Supplementary Fig. S4D and 4E), and observed they have chromatin and histone binding properties and has a role in DNA replication-independent chromatin assembly. Further, we conducted GOB network analysis of DEPP, including CSe1, smarcd1, Hk2, Pkm, Tfpt, Tcof1, champ1, nasp, Macf1, Hat1, Bcam, Atrx, Nmd3, Sde2, Ubr4, Hsph1, Trap1, nucks, Cdk1, Mki67, Tpx2, champ1 (S1_Supplementary Fig. 4F), and observed that they exhibit cross-talk in the kinetochore process, chromatin condensation, nuclear division, mitotic cell cycle, and chromatin remodelling. We have also detected some DEPP, including Cdk1, Mki67, Nucks1,

and Tpx2, crucial for mitotic cell division and mitochondrial ATP synthesis through GOB network analysis, implicating their role in G2/M cell cycle arrest and oxidative phosphorylation (S1_Supplementary Fig. S5A and 5B). However, further studies are needed to confirm the role of Ca^{2+} in the regulation of above processes in mESCs.

Discussion

In recent years, pluripotent stem cells have received extensive importance in the field of regenerative medicine to study cell development and differentiation. However, the role of Ca^{2+} signalling in the maintenance of pluripotency is not yet explored. Previous work in drosophila, mesenchymal stem cells and mESCs has demonstrated that stem cells undergo differentiation upon Ca^{2+} reduction (Shim et al., 2013, Vallet et al., 2025, MacDougall et al., 2025, Zhu and Zhang 2019, Apáti et al., 2016). Our study showed that low calcium leads to the spontaneous differentiation of mESCs, reflecting the broadly conserved phenomenon in stem/progenitor cells across the species. In stem cell biology, there is a persistent effort to understand the mechanism underlying ESC pluripotency. Nevertheless, the comprehensive repertoire of molecules involved in controlling the ESC state is not yet completely understood. Several studies have reported the heterogeneous expression of Nanog in mESCs but the mechanism underlying the same is still unclear (Torres-Padilla and Chambers 2014). Previous finding in hESCs has also indicated the heterogenous expression of Ca^{2+} signalling in hESCs (Huang et al., 2017). Our data indicates a correlation between the heterogenous expression of Oct4 and Nanog with the heterogeneous level of Ca^{2+} and pCaMKIIα in mESCs, which suggest that calcium might be related with the heterogenous expression of pluripotency markers. Earlier reports have suggested that activation of calcium receptor RyR2, calcium-sensing receptor (CaSR) and increasing calcium level promotes the

differentiation of human and mouse ESCs towards cardiac differentiation (Meng et al., 2025, Sun et al., 2013). Interestingly, we noted that upon Ca^{2+} reduction, mESCs showed the mESCs tendency to differentiate towards mesoderm lineage, suggesting that Ca^{2+} signalling might be important in undifferentiated mESCs to mask the expression of mesoderm markers. Furthermore, our data signifies the role of high Ca^{2+} in mediating the degradation of brachyury protein, and low calcium and low pUBQ proteasomal system for its stability, which also suggests the activation of other signalling pathways upon calcium reduction to determine lineage specificity. Moreover, our data demonstrate that calcium might not be controlling LIF-JAK-STAT3 pathway for the regulation of core pluripotency and differentiation markers and has no role at the transcriptional level but controls the stability of these fundamental regulators at the post-translational level. Our pCaMKIIα KD data indicate that pCaMKIIα is important for the stability of Oct4 and Nanog proteins in mESCs. We have also observed the co-localization of Oct4 and pCaMKIIα, but have not checked whether and how pCaMKIIα phosphorylates core pluripotency markers Oct4 and Nanog and how it results in their downregulation. It is well known that pCaMKIIα is a serine-threonine kinase and is involved in the phosphorylation of a wide array of proteins (Clapham 2007), thus suggesting that it might have a role in regulating the phosphorylation status of these core pluripotency markers. Earlier studies have demonstrated that phosphorylation of Oct4 and Nanog proteins at serine residues decreases their stability and dispenses them towards the pUBQ-mediated proteasomal degradation pathway in mESCs (Bae et al., 2017, Kim et al., 2014). Our data demonstrate that Ca^{2+} might be regulating the stability of Oct4 and Nanog proteins independent of the pUBQ system. Several reports suggest that protein degradation can happen independent of polyubiquitin tagging or without the 19S proteasome subunit by 20S or 26S mediated proteolysis through structural disorder (Shang and Taylor 2011, Ben-Nissan and Sharon 2014). Previous findings have advocated that Ca^{2+} and Ca2+-binding proteins

promote conformational change upon binding to target proteins and modulate their activity and stability (Clapham, 2007, . Strynadka, and James, 1991, Hołubowicz et al., 2017) Therefore, further structural, biochemical, and molecular studies are needed to understand the in-depth mechanism of how Ca^{2+} regulate the activity and stability of pluripotency markers either through phosphorylation at specific residues or conformational change and structural disorder.

Interestingly, our data also signifies that Ca^{2+} has a role in controlling the expression of p-bodies and stress granule markers, but has no role in controlling the expression of pluripotency and differentiation markers at a post-transcriptional level, which indicates that Ca^{2+} might be regulating other signalling pathways at the post-transcriptional level important for the maintenance of pluripotency of mESCs. Our data demonstrate that 3'UTR-mediated NMD is important for the maintenance of pluripotency, while the splicing-dependent NMD mechanism is more active during the differentiation process, which signifies that Ca^{2+} plays a role in the modulation of different post-transcriptional processes. Our data has identified several RNA-binding and ribosomal PP including edc4, dcp1a, xrn1, tudor, Pa2g4, Nmd3, Ddx21, Srsf5, Srsf6, Srsf1, EDC4, Fkbp4, Cpsf3, Fip1l1, Hnrnpab, Hnrnpa, Hnrnpa3, Rbm39, Dhx15, Acin1, Snw1, Larp, Srrm1, Clasrp, Rps18, Rars, Eif3c, Eef1a1, Eif5a, Rpl18a, Eif2s1, Rpl5, Rps8, Rplp2, Rpl34, Eef1d, Rpl27, Eif3b, Rpl23a implicated in mRNP complex formation, alternative splicing, alternative polyadenylation, mRNA stability, 5′TOP mRNAs stability, miRNA biogenesis, mRNA decapping and NMD through GOB analysis and literature review (Martinez et al., 2013, Hochstoeger et al., 2024, Chiang et al., 2013, Decker and Parker, 2012), which suggests a widespread role of Ca^{2+} at a post-transcriptional level rather than global translational control. Our data have revealed decreased expression of

dcp1a, tudor, and xrn1 and increased expression of edc4 upon Ca^{2+} reduction, which signifies differential expression of p-bodies markers upon Ca^{2+} manipulation. Moreover, our data indicate that pCaMKIIα is also a part of p-bodies component machinery, which suggests that Ca^{2+} might be regulating the dynamic, composition, interaction, and activity of p-bodies markers through regulating their phosphorylation status. Chiang et al. have revealed that edc4 binding to dcp1a is independent of its phosphorylation status, while the phosphorylation status of dcp1a is important for its strong binding to dcp2 (decapping co-factor) (Chiang et al., 2013). Moreover, studies on yeast demonstrated that Ca^{2+} is required for p-bodies formation and disclosed variations in the size of p-body granules (Kilchert et al., 2010, Park et al., 2016). Park et al. also observed co-localization of calcineurin (calcium-calmodulin-activated serine/threonine-specific phosphatase) with p-bodies and stress granules markers in yeast (Park et al., 2016). Taken together, our data and these studies indicate that Ca^{2+} might have a role in mediating the interaction of dcp1a with other p-bodies and stress granule markers and the formation of mRNP granule composition through regulating phosphorylation and dephosphorylation. Therefore, further detailed studies are needed to elucidate the role of Ca^{2+} in the regulation of mRNP granule composition in undifferentiated and differentiated mESCs.

In our phosphoproteomic data, we have observed the upregulation of Atp5f1a, Cox4i1, Hk2, and the downregulation of Pkm upon Ca^{2+} reduction, which are important for oxidative phosphorylation and mitochondrial fusion (Lis et al., 2016, Li et al., 2019, Čunátová et al., 2021). It has already been reported that undifferentiated ESCs have globular immature mitochondria and prefer glycolysis over oxidative phosphorylation, whereas during differentiation, mitochondria undergo conformation change and differentiated cells favour

oxidative phosphorylation for energy production (Fu et al., 2019). Our data also suggest globular mitochondria in undifferentiated mESCs and long tubular mitochondria, as well as an increase in the number of mitochondria upon Ca^{2+}reduction in mESCs, which illustrates that low calcium might be needed for mitochondrial morphological remodelling and further studies are needed to examine the role of Ca^{2+}in mitochondrial biogenesis and metabolic switching in mESCs.

Furthermore, we have not observed any apoptosis in mESCs upon bapta treatment, nor did mESCs show any stress-related phenotype. Indeed, our phosphoproteomic data detected apoptosis marker BCL-2-associated transcription factor 1, but we have not observed any significant change in its protein profile (S2_Supplementary Table 1), which indirectly supports that apoptosis might not be dysregulated. In addition, we have also not observed any ER stress-related key phosphoproteins such as PERK, eIF2α, and IRE1α (Chen et al., 2023) in our phosphoprotein dataset (S2_Supplementary Table 1). Moreover, ER stress triggers heat shock protein response (Liu and Chang 2008). We have detected several heat shock phosphoproteins, such as HSP-90 alpha, HSP 90 beta, Hspa8, Hspa4, Hspb1, Ahsa1, Hsph1, and Carhsp1 in our phosphoproteomic dataset (S2_Supplementary Table 1). Among these, Hspa8 and Hsph1 were only significantly upregulated and downregulated, which indicates that ER stress might not be majorly altered.

Taken together, our data indicate that calcium might be having a broad role in modulating various biological processes such as cell cycle arrest, protein stability, RNA splicing, mRNA stability, ribosome biogenesis, mRNP granule formation, ubiquitination, metabolism,

telomere maintenance, oxidative phosphorylation, mitochondrial biogenesis, chromatin regulation, RNA polyadenylation for the maintenance of mESCs identity.

Materials and Methods

Culturing of mESCs and calcium modulation

mESCs E14TG2a and E14 cell lines were maintained on 0.1% gelatin at 37 ^{o}C in a 5% CO2 incubator in ES medium containing high glucose DMEM (GibcoTM), ESGRO recombinant mouse LIF, 15% ES cell FBS (GibcoTM), β-Mercaptoethanol (GibcoTM), 1x NEAA (GibcoTM), and gentamycin (GibcoTM). To induce spontaneous differentiation, mESCs were trypsinized with 0.05% Trypsin-EDTA (GibcoTM) and cultured in ES media in the absence of LIF. For Bapta (InvitrogenTM) and thapsigargin treatment, mESCs were cultured in the presence of LIF with different concentrations of bapta (1μM and 2μM) and thapsigargin (250pm, 500pm, and 1nM) for 72 hours. Bapta and thapsigargin stock solutions were prepared using DMSO. An equal amount of DMSO was added to the control media as compared to bapta and thapsigargin. The medium was changed every day. All experiments were done at 72 hour time interval except few such as mitochondrial staining was done at 48 hours where mitochondrial morphological change was detected early and transcript profile was studied at 48 hours and 4 days to ascertain transcript are unchanged upon calcium manipulation at shorter and longer time interval and cell cycle, proliferation and cMyc staining was studied for 5 days with 72 hour bapta treatment and 48 hour rescue condition.

Cell proliferation assay

mESCs proliferation was calculated using the trypan blue method, and cell cycle analysis was done by PI staining. Briefly, mESCs were fixed in 70% ethanol and stored at -20 °C. Fixed cells were centrifuged at 1000 rpm for 3-5 min and washed with PBS 2-3 times and PI staining solution (80 μg/ml PI, 100 μg/ml RNase A and 0.1 % Triton X-100) for 7 hrs at 4 °C. After incubation, mESCs were washed with PBS 2-3 times and cell cycle analysis was done by using flow cytometry and BD software.

Mitotracker-red staining, Fluo4 staining, lysotracker Staining, and Immunofluorescence staining

Cells were grown on coverslips in ES media containing bapta (2μM) and thapsigargin (1nM). After 72 hours, cells were incubated with media containing Fluo4 (1μM), lysotracker (100nM), and mitotracker red (100nM) for 45 minutes, followed by 2-3 washes with media and immediately taken for live cell imaging. In the case of Fluo 4 staining, cells were incubated at 37 °C in a 5% CO2 incubator for 15 minutes before live cell imaging. The imaging was done using a confocal microscope at 40x magnification. For immunostaining, cells were grown on coverslips and treated with bapta (2 μM) and thapsigargin (1nM) for 72 hours, followed by fixation in 4% paraformaldehyde (PFA) overnight at 4 °C. After incubation, PFA was removed and cells were washed with PBS twice. The fixed cells were permeabilised using 0.4% Triton X-100 for 2 hours at room temperature (RT). Then the cells were blocked using the blocking buffer (5% BSA and 0.1% Tween-20 in PBS) for 2 hrs at RT. After blocking, cells were incubated with primary antibodies at 4 °C overnight or 3 hours at RT, followed by twice washing with PBS for 5 minutes each. The primary antibodies used were OCT3/4 (Invitrogen), Nanog (Invitrogen), elf41a (Abcam), DCP1a (sigma), XRN1, beta-actin (mRNP) (Santacruz), pCAMKIIα (Cell Signalling Technology), pSTAT3

(Abcam), cmyc (Abcam), and Brachyury. Further, secondary antibodies (Jackson Immunoresearch Laboratories (West Grove, PA) were added and incubated for 1-2 hr at RT. After incubation, cells were washed with PBS twice for 5 minutes and mounted on a glass slide using mounting media containing DAPI. For IF experiments, confocal images were used for calculating mean intensity using ImageJ software for the gene expression analysis.

Gene expression analysis

RNA was extracted using the Trizol (Invitrogen, Carlsbad, CA, USA) method. Briefly, cells were lysed and homogenised using Trizol, and 1/5 volume of chloroform was added to the Trizol to extract RNA by centrifuging at 12000 rpm at 4 °C for 20 mins. After centrifugation, an aqueous layer was collected, and an equal volume of isopropanol was added, and samples were incubated at -80 oC overnight. After incubation, samples were centrifuged to precipitate RNA. After centrifugation, precipitated RNA was washed with 70% ethanol, dried, and dissolved in nuclease-free water and stored at -80°C. Further, 1 μg of RNA was reverse transcribed with Superscript II or Superscript III reverse transcriptase (Invitrogen) according to the manufacturer's protocol. Real-time polymerase chain reaction (PCR) was performed using AB Invitrogen with Power Sybr Green (Thermo Fisher Scientific) according to the manufacturer's instructions. The gene expression analysis of pluripotency and differentiation markers was calculated using the formula 2=ΔΔct and normalised to glyceraldehyde 3 phosphate (GAPDH).

Protein extraction and western blotting

For protein extraction, mESCs were lysed using radioimmunoprecipitation buffer (RIPA buffer). The samples were then centrifuged at 12000 rpm for 10 minutes at 4 ^{o}C. The supernatant was collected, and protein estimation was quantified by the Bradford method using BSA as a standard. An equal amount of proteins (5-10 μg) was separated on a 12% SDS-PAGE gel. Proteins were electrophoretically transferred into polyvinylidine difluoride membranes (Bio-Rad) for western blot analysis. The blots were blocked with blocking buffer containing 5% BSA in TBST (20mM Tris pH 7.5, 150mM NaCl, and 0.1% Tween-20) followed by incubation with primary antibody at 4 ^{o}C overnight or 3-4 hours at RT. After incubation, blots were washed twice with TBST, and membranes were incubated with horseradish peroxidase (HRP)-conjugated secondary antibody for 2 hrs. Signals were detected with ECL substrate (Amersham GE) using ImageQuant. The primary antibodies used were OCT3/4 (Invitrogen), Nanog (Invitrogen), GAPDH (Invitrogen), cMyc (Abcam), and pSTAT3 (Abcam), and secondary antibodies were anti-rabbit HRP and anti-goat HRP. GAPDH was used as a loading control.

Cycloheximide chase assay, MG132 treatment for analysing protein stability, and actinomycin D and CHX assay for posttranscriptional activity detection

mESCs were cultured in the absence and presence of B 2μM for 72hrs, followed by treatment with 50ug/ml CHX for 1hr, and protein levels of Oct4 and Nanog were detected every 20 min using western blot. For the MG132 experiment, mESCs were cultured in the absence and presence of bapta (2uM) for 72 hours, followed by 10uM MG132 treatment for 1 1hr and detected using western blot and IF. For posttranscriptional analysis of pluripotency markers, mESCs were treated with 5ug/ml of actinomycin D (ACD) and CHX (50ug/ml) for 2 hr after

culturing the mESCs in C+L, B2uM, T1nM, C-L, C-LT1nM, and samples were extracted in Trizol for RNA purification.

Electroporation

Electroporation was performed using an Invitrogen Neon Transfection System (100ul) according to the manufacturer's instructions. Briefly, mESCs were trypsinized and washed with PBS and centrifuged at 1000rpm for 3-5 min. The mESCs pellet was then re-suspended in the resuspension buffer (Buffer R) containing the required plasmid (pCAMKIIa shRNA, SERCA shRNA, Design 1 Endoplasmic reticulum (D1ER) calcium sensor for measuring endoplasmic reticulum calcium as described by Waldeck-Weiermair et al., (2015), and NMD reporter plasmids [NMD reporter plasmids were kind from Konstantin A. Lukyanov from Sergey A. Lukyanov lab, Russian Academy of Sciences, Russia]). Further, electroporation was performed using a parameter of 900 volts, 3 pulses, 23 width. After electroporation, mESCs were immediately transferred into the ES media without antibiotics and incubated at 37 ^{o}C in a 5% CO2 incubator. Fresh media containing antibiotics was added after 24 hours, and GFP expression was analysed between 48 hours and 72 hours. After 48 hours, mESCs were collected in RIPA buffer for western blot, TRIzol for RNA extraction and fixed in 4% for immunofluorescence staining.

Polysome profiling

mESCs were cultured in the presence of B2μM for 72hour and pellet was resuspended in polysome lysis buffer (20mM Tris pH-7.4, 200mM KCL, 5mM Mgcl2, 0.7% triton X-100, 1x protease inhibitor, RnaseoOUT, 100ug/ml CHX, 1mM DTT). A 15-45% sucrose gradient

was prepared in gradient buffer (20mM Tris, pH 7.4, 5mM MgCl2, 100mM KCL, 1mM DTT, 100 μg/ml CHX) using a gradient mixer. An equal amount of RNA/260OD was loaded into the gradient and centrifuged at 39000 rpm at 4 ^{o}C for 2.5 hr. Polysome peak was analysed using polysome profiler, and cytoplasmic mRNP granule, 80s ribosome, and polysome fractions were collected in absolute ethanol. Samples were stored at -80 ^{o}C overnight, and RNA isolation was performed by collecting pellets from ethanol fractions in Trizol or by using an RNA extraction kit (Qiagen). cDNA synthesis was carried out using Superscript II or Superscript III according to the manufacturer's instructions.

Phosphoproteomics

Phosphoproteomics experiment was conducted n=2 times. mESCs were collected from one 60mm dish and one 35mm dish, each dish cultured on different days and pooled to form one set. mESCs were cultured for 72 hours in the presence of B 2μM, and proteins were extracted using RIPA buffer containing protease and phosphatase inhibitors. Further, Proteins were precipitated using 15% TCA followed by a 90% acetone wash. The protein pellet was dissolved in 8% urea buffer (8% urea in 100mM ammonium bicarbonate buffer) containing 5 mM DTT, 1x phosphor stop inhibitor and incubated at RT for 35 min for complete denaturation of proteins. Protein levels were estimated using the Bradford method. Equal amounts of proteins (500ug and 200ug) were taken for control and bapta-treated samples and incubated at 56 ^{o}C for 45 min with 5mM DTT concentration. Further samples were treated with 10mM iodoacetamide and incubated at 56 ^{o}C for 45 min. After incubation, Samples were diluted 10 times with ammonium bicarbonate buffer and incubated at 37 °C overnight with trypsin gold (mass spec grade, Promega) in a 1:100 ratio. After incubation, peptides were collected using 1% FA. Alternatively, during standardization of protocol, the remaining

protein pellet after first digestion was again dissolved twice in ammonium bicarbonate buffer to re-activate trypsin gold and supplemented with 500ng trypsin gold and incubated at 37 °C for 8-9 hrs, and overnight respectively, and peptides were collected using 1% formic acid. Peptides were purified using the Oasis HLB column according to manufacturer instructions (Waters). The eluted peptides were dried using a speed vacuum. Dried peptides were resuspended in 50% acetonitrile in 0.2% formic acid, and phosphopeptide enrichment was done using Fe-NTA resin. Peptides were incubated in Fe-NTA for 3-4 hrs and washed twice with 50% acetonitrile containing 0.2% formic acid. Finally, phosphopeptides were eluted using a 2.5% ammonium hydroxide buffer. An equal amount of phosphopeptides was used in LC/MS/MS analysis using the Thermo Orbitrap Fusion system. Fe-NTA resin was prepared by chelating Ni-NTA resin according to the method described by Sanford & Smolka, 2021 with slight modification. After mass spec analysis, raw data of phosphopeptides were analysed by Proteome Discoverer software from Thermo Fischer Scientific with standardised consensus and processing workflow parameters with slight modifications, including s/n ratio 5, threshold 50, unique peptides, static carbamidomethylation modification (+57.021 Da), and phosphosites detection was done by selecting dynamic phosphorylation modification for serine-threonine and tyrosine. Further log2fold change was calculated from abundance values detected by the software, and p-value was calculated using the one-way Chi-square test. The heat map was plotted for significantly differentially regulated genes using an SR plot web server as described by Tang et al., 2023.

Statistical analysis: p-value calculated by the two-sample t-test method from the mean and standard deviation as described by Xu et al. (2017) using MedCalc online statistical software calculator (MedCalc Software, 2024).

Author contributions

TM initiated the project. TM and SS have designed the experiments and performed the analysis. DP has given suggestions on p-body markers. SS performed all the experiments and wrote the manuscript with input from all authors.

Acknowledgements:

The work was supported by the inStem core funds.

Resource availability: Further information and requests for reagents may be directed to and will be fulfilled by the Shikha Sharma **(**shikha.ss19254@gmail.com**)**

Materials availability

This study did not generate new unique reagents.

Funding declaration

This work has not received any specific funding.

Declaration of interests

The authors declare no competing interests

References

1. Apáti Á, Berecz T, Sarkadi B (2016) Calcium signaling in human pluripotent stem cells. Cell Calcium 59(2-3):117-23.
2. Bae KB, Yu DH, Lee KY, Yao K, Ryu J, Lim DY, Zykova TA, Kim MO, Bode AM, Dong Z (2017) Serine 347 Phosphorylation by JNKs Negatively Regulates OCT4 Protein Stability in Mouse Embryonic Stem Cells. Stem Cell Reports 9:2050-2064.
3. Ben-Nissan G, Sharon M (2014) Regulating the 20S proteasome ubiquitin-independent degradation pathway. Biomolecules 4:862-84.
4. Berridge MJ, Bootman MD, Roderick HL (2003) Calcium signalling: dynamics, homeostasis and remodelling. Nat Rev Mol Cell Biol. 4:517-529.
5. Chen X, Shi C, He M, Xiong S, Xia X (2023) Endoplasmic reticulum stress: molecular mechanism and therapeutic targets. Signal Transduct Target Ther 8(1):352.
6. Chi M, Evans H, Gilchrist J, Mayhew J, Hoffman A, Pearsall EA, Jankowski H, Brzozowski JS, Skelding KA (2016) Phosphorylation of calcium/calmodulin-stimulated protein kinase II at T286 enhances invasion and migration of human breast cancer cells. Sci Rep 6:33132.
7. Chiang PY, Shen YF, Su YL, Kao CH, Lin NY, Hsu PH, Tsai MD, Wang SC, Chang GD, Lee SC, Chang CJ (2013). Phosphorylation of mRNA decapping protein Dcp1a by the ERK signaling pathway during early differentiation of 3T3-L1 preadipocytes. PLoS One. 8, e61697.
8. Clapham DE (2007) Calcium signalling. Cell 131:1047-1058.

9. Collatz MB, Rüdel R, Brinkmeier H (1997) Intracellular calcium chelator BAPTA protects cells against toxic calcium overload but also alters physiological calcium responses. Cell Calcium 21:453-9.
10. Čunátová K, Reguera DP, Vrbacký M, Fernández-Vizarra E, Ding S, Fearnley IM, Zeviani M, Houštěk J, Mráček T, Pecina P (2021) Loss of COX4I1 Leads to Combined Respiratory Chain Deficiency and Impaired Mitochondrial Protein Synthesis. Cells 10(2): 369.
11. Czechanski A, Byers C, Greenstein I, Schrode N, Donahue LR, Hadjantonakis AK, Reinholdt LG (2014) Derivation and characterization of mouse embryonic stem cells from permissive and nonpermissive strains. Nat Protoc. 9:559-74.
12. Decker CJ, Parker R (2012) P-bodies and stress granules: possible roles in the control of translation and mRNA degradation. Cold Spring Harb Perspect Biol. 4(9): a012286.
13. Fagnocchi L, Cherubini A, Hatsuda H, Fasciani A, Mazzoleni S, Poli V, Berno V, Rossi RL, Reinbold R, Endele M, Schroeder T, Rocchigiani M, Szkarłat Ż, Oliviero S, Dalton S, Zippo A (2016). A Myc-driven self-reinforcing regulatory network maintains mouse embryonic stem cell identity. Nat Commun. 7:11903.
14. Fu W, Liu Y, Yin H (2019) Mitochondrial Dynamics: Biogenesis, Fission, Fusion, and Mitophagy in the Regulation of Stem Cell Behaviors. Stem Cells Int 2019:9757201.
15. Ghimire S, Van der Jeught M, Neupane J, Roost MS, Anckaert J, Popovic M, Van Nieuwerburgh F, Mestdagh P, Vandesompele J, Deforce D, Menten B, Chuva de Sousa Lopes S, De Sutter P, Heindryckx B (2018) Comparative analysis of naive, primed and ground state pluripotency in mouse embryonic stem cells originating from the same genetic background. Sci Rep 8:5884.

16. Hirst NL, Lawton SP, Walker AJ (2022) CaMKII regulates neuromuscular activity and survival of the human blood fluke Schistosoma mansoni. Sci Rep 12(1):19831.
17. Hochstoeger T, Papasaikas P, Piskadlo E, Chao JA (2024) Distinct roles of LARP1 and 4EBP1/2 in regulating translation and stability of 5'TOP mRNAs. Sci Adv 10(7):eadi7830.
18. Hołubowicz R, Wojtas M, Taube M, Kozak M, Ożyhar A, Dobryszycki P (2017) Effect of calcium ions on structure and stability of the C1q-like domain of otolin-1 from human and zebrafish. FEBS J 284:4278-4297.
19. Huang Jj, Wang Yj, Zhang M, Zhang P, Liang H, Bai HJ, Yu XJ, Yang HT (2017) Functional expression of the Ca^{2+} signaling machinery in human embryonic stem cells. Acta Pharmacol Sin 38:1663–1672.
20. Kao SH, Wang WL, Chen CY, Chang YL, Wu YY, Wang YT, Wang SP, Nesvizhskii AI, Chen YJ, Hong TM, Yang PC (2015) Analysis of Protein Stability by the Cycloheximide Chase Assay. Bio Protoc. 5:e1374.
21. Kilchert C, Weidner J, Prescianotto-Baschong C, Spang A (2010) Defects in the secretory pathway and high Ca2+ induce multiple P-bodies. Mol Biol Cell 21(15): 2624-38.
22. Kim SH, Kim MO, Cho YY, Yao K, Kim DJ, Jeong CH, Yu DH, Bae KB, Cho EJ, Jung SK, Lee MH, Chen H, Kim JY, Bode AM, Dong Z (2014) ERK1 phosphorylates Nanog to regulate protein stability and stem cell self-renewal. Stem Cell Res 13:1-11.
23. Kobayashi H, Kikyo N (2015) Epigenetic regulation of open chromatin in pluripotent stem cells. Transl Res 165:18-27.
24. Li T, Han J, Jia L, Hu X, Chen L, Wang Y (2019) PKM2 coordinates glycolysis with mitochondrial fusion and oxidative phosphorylation. Protein Cell 10:583-594.

25. Lis P, Dyląg M, Niedźwiecka K, Ko YH, Pedersen PL, Goffeau A, Ułaszewski S (2016) The HK2 Dependent "Warburg Effect" and Mitochondrial Oxidative Phosphorylation in Cancer: Targets for Effective Therapy with 3-Bromopyruvate. Molecules. 21(12): 1730.
26. Liu Y, Chang A (2008) Heat shock response relieves ER stress. EMBO J 27(7):1049-59.
27. Lytton J, Westlin M, Hanley MR (1991) Thapsigargin inhibits the sarcoplasmic or endoplasmic reticulum Ca-ATPase family of calcium pumps. J Biol Chem 266:17067-71.
28. MacDougall MS, Clarke R, Merrill BJ (2019) Intracellular Ca^{2+} Homeostasis and Nuclear Export Mediate Exit from Naive Pluripotency. Cell Stem Cell 25(2):210-224.
29. Martinez NJ, Chang HM, Borrajo Jde R, Gregory RI (2013) The co-chaperones Fkbp4/5 control Argonaute2 expression and facilitate RISC assembly. RNA 19(11):1583-93.
30. MedCalc Software Ltd. Comparison of means calculator. https://www.medcalc.org/calc/comparison_of_means.php (Version 23.0.1; accessed August 22, 2024)
31. Mège RM, Ishiyama N (2017) Integration of Cadherin Adhesion and Cytoskeleton at Adherens Junctions. Cold Spring Harb Perspect Biol 9(5):a028738.
32. Meng Y, Deng C, Xiao X, Wei S, Song C, Wang J, Lei CL, Liu W, Chen G (2025) The modulation of calcium and chloride channels induces cardiomyocytes from human pluripotent stem cells. Int J Biol Sci 21(1):95-108.
33. Moore CB, Guthrie EH, Huang MT, Taxman DJ (2010) Short hairpin RNA (shRNA): design, delivery, and assessment of gene knockdown. Methods Mol Biol 629:141-58.

34. Moore JL, Bhaskar D, Gao F, Matte-Martone C, Du S, Lathrop E, Ganesan S, Shao L, Norris R, Sanz NC, Annusver K, Kasper M, Cox A, Hendry C, Rieck B, Krishnaswamy S, Greco V (2024) Correction: Cell cycle controls long-range calcium signaling in the regenerating epidermis. J Cell Biol 223(4):e20230209503052024c. Erratum for: J Cell Biol. 2023 Jul 3;222(7):e202302095.
35. Ohtsuka S, Nakai-Futatsugi Y, Niwa H (2015) LIF signal in mouse embryonic stem cells. JAKSTAT 4(2):e1086520.
36. Park HS, Chow EW, Fu C, Soderblom EJ, Moseley MA, Heitman J, Cardenas ME (2016) Calcineurin Targets Involved in Stress Survival and Fungal Virulence. PLoS Pathog 12(9):1005873.
37. Park JH, Chung CG, Park SS, Lee D, Kim KM, Jeong Y, Kim ES, Cho JH, Jeon YM, Shen CJ, Kim HJ, Hwang D, Lee SB (2020) Cytosolic calcium regulates cytoplasmic accumulation of TDP-43 through Calpain-A and Importin α3. Elife 9:e60132.
38. Pereverzev A, Gurskaya N, Ermakova GV, Kudryavtseva EI, Markina NM, Kotlobay AA, Lukyanov SA, Zaraisky AG, Lukyanov KA (2015) Method for quantitative analysis of nonsense-mediated mRNA decay at the single cell level. Sci Rep 5:7729.
39. Ruan Y, He J, Wu W, He P, Tian Y, Xiao L, Liu G, Wang J, Cheng Y, Zhang S, Yang Y, Xiong J, Zhao K, Wan Y, Huang H, Zhang J, Jian R (2017) Nac1 promotes self-renewal of embryonic stem cells through direct transcriptional regulation of c-Myc. Oncotarget 8(29):47607-47618.
40. Sanford EJ, Smolka MB (2021) Fe-NTA Microcolumn Purification of Phosphopeptides from Immunoprecipitation (IP) Eluates for Mass Spectrometry Analysis. Bio Protoc. 11(15):e4113.
41. Schwirtlich M, Emri Z, Antal K, Mate Z, Katarova Z, Szabo G (2010) GABA(A) and GABA(B) receptors of distinct properties affect oppositely the proliferation of mouse

embryonic stem cells through synergistic elevation of intracellular Ca(2+). FASEB J 24:1218–1228.

42. Scognamiglio R, Cabezas-Wallscheid N, Their MC, Altamura S, Reyes A, Prendergast ÁM, Baumgärtner D, Carnevalli LS, Atzberger A, Haas S, von Paleske L, Boroviak T, Wörsdörfer P, Essers MA, Kloz U, Eisenman RN, Edenhofer F, Bertone P, Huber W, van der Hoeven F, Smith A, Trumpp A (2016) Myc Depletion Induces a Pluripotent Dormant State Mimicking Diapause. Cell 164(4):668-80.
43. Shang F, Taylor A (2011) Ubiquitin-proteasome pathway and cellular responses to oxidative stress. Free Radic Biol Med 51:5-16.
44. Shim J, Mukherjee T, Mondal BC, Liu T, Young GC, Wijewarnasuriya DP, Banerjee U (2013) Olfactory control of blood progenitor maintenance. Cell 155:1141-53.
45. Sim YJ, Kim MS, Nayfeh A, Yun YJ, Kim SJ, Park KT, Kim CH, Kim KS (2017) 2i Maintains a Naive Ground State in ESCs through Two Distinct Epigenetic Mechanisms. Stem Cell Reports. 8:1312-1328.
46. Strynadka NCJ, and James MNJ (1991) Towards an understanding of the effects of calcium on protein structure and function. Current Opinion in Structural Biology 1: 905-914.
47. Sun J, He W, Bai SZ, Peng X, Zhang N, Li HX, Zhang WH, Wang LN, Shao XQ, He YQ, Yang GD, Wu LY, Wang R, Xu CQ (2013) The expression of calcium-sensing receptor in mouse embryonic stem cells (mESCs) and its influence on differentiation of mESC into cardiomyocytes. Differentiation. 5(1-2):32-40.
48. Tang Y, Tian XC (2013) JAK-STAT3 and somatic cell reprogramming. JAKSTAT 2:e24935.

49. Tang D, Chen M, Huang X, Zhang G, Zeng L, Zhang G, Wu S, Wang Y (2023) SRplot: A free online platform for data visualization and graphing. PLoS One 18:e0294236.

50. Todorova MG, Fuentes E, Soria B, Nadal A, Quesada I (2009) Lysophosphatidic acid induces Ca2+ mobilization and c-Myc expression in mouse embryonic stem cells via the phospholipase C pathway. Cell Signal 21:523–528.

51. Torres-Padilla ME, Chambers I (2014) Transcription factor heterogeneity in pluripotent stem cells: a stochastic advantage. Development 141(11):2173-81.

52. Vallet L, Sánchez-Petidier M, Fernandes R, Naumova N, Merla C, Consales C, Innamorati G, André FM, Mir LM (2025) Calcium oscillations in mesenchymal stem cells, a control on cell cycle progression to influence cell fate towards proliferation or differentiation?. Stem Cell Res Ther 16:446.

53. Waldeck-Weiermair M, Bischof H, Blass S, Deak AT, Klec C, Graier T, Roller C, Rost R, Eroglu E, Gottschalk B, Hofmann NA, Graier WF, Malli R (2015) Generation of Red-Shifted Cameleons for Imaging Ca^{2+} Dynamics of the Endoplasmic Reticulum. Sensors (Basel) 15(6):13052-68.

54. Wang D, Xu Q, Yuan Q, Jia M, Niu H, Liu X, Zhang J, Young CY, Yuan H (2019) Proteasome inhibition boosts autophagic degradation of ubiquitinated-AGR2 and enhances the antitumor efficiency of bevacizumab. Oncogene 38:3458–3474.

55. Xu M, Fralick D, Zheng JZ, Wang B, Tu XM, Feng C (2017) The Differences and Similarities Between Two-Sample *T*-Test and Paired *T*-Test. Shanghai Arch Psychiatry 29(3):184-188..

56. Yanagida E, Shoji S, Hirayama Y, Yoshikawa F, Otsu K, Uematsu H, Hiraoka M, Furuichi T, Kawano S (2004) Functional expression of Ca2+ signalingpathwaysin mouse embryonic stem cells. Cell Calcium 36:135–146.

57. Ye Y, Xie W, Ma Z, Wang X, Wen Y, Li X, Qi H, Wu H, An J, Jiang Y, Lu X, Chen G, Hu S, Blaber EA, Chen X, Chang L, Zhang W (2024) Conserved mechanisms of self-renewal and pluripotency in mouse and human ESCs regulated by simulated microgravity using a 3D clinostat. Cell Death Discov. 10, 68.
58. Yeo JC and Ng HH (2013) The transcriptional regulation of pluripotency. Cell Res. 23, 20-32.
59. Zhu Y, Zhang J Calcium: (2019). A New Guardian of Naive Pluripotency. Cell Stem Cell. 25(2), 169-170.

Figure Legends

Figure 1: Calcium level in mESCs: A) Fluo4 staining, B) DIER reporter expression, C) Fluo4 and lysotracker staining of mESCs under different conditions (C+L, B2uM, T1nM, C-L, C-L+T1nM) (n=3-5).

D and E) Bar plot represents the mean intensity of fluo4 staining and D1ER reporter in mESCs calculated from the confocal images of the above experiments.

F) Bar graph showing the percentage of the proliferation of mESCs treated with B1uM, B2uM, and B5uM for 72 hrs compared to control using the trypan blue method (n=4).

G) Bar graph showing percentage of the proliferation of mESCs treated with B2uM and B5uM for 5 days and B2R condition compared to control D2 and D5 respectively (n=4)

H) Western blot detection of cMyc in the presence and absence of B2uM for 72hrs (n=2)

I) Immunofluorescence (IF) detection of cMyc expression in mESCs in the presence of B2uM for 5 days and B2R condition (n=3)

J) The bar plot represents the mean intensity of cMyc expression calculated from the confocal images of the above experiments.

K) QPCR of cMyc expression in mESCs treated with B2uM for 72hrs (n=3).

L) Cell cycle analysis of control (D2) and B2uM treated mESCs for 72 hrs (n=4). Significant p-value (0.0085) was detected for B2/D2 (G2/M)

M) Cell cycle analysis of D2, B2uM treated mESCs for 5 days and B2R condition (n=5). Significant p-value (0.0003 and 0.01) was detected for B2/D2 and B2R/B2 (G2/M)

C+L= Control media + Lif; B1uM= C+L + Bapta 1uM; B2uM = C+ L + Bapta 2uM; T1nM= C+L + thapsigargin 1nM; C-L= control media without Lif; C-L+T1nM = C-L + thapsigargin 1nM; D2= C+L+ dmso equivalent to B2uM condition; B5uM = C+L+ Bapta 5uM; D5= C+L+ dmso equivalent to B5uM condition, B2R= B2 media for 72 hour + D2 media for 48 hour

The mean intensity was calculated from the confocal images for all experiments using ImageJ software. p-value representation with asterisk <0.05 (*), <0.01 (**), <0.001 (***), <0.0001 (****).

Figure 2: Role of calcium in pluripotency: IF detection of **A)** Nanog (red), **B)** Oct4 (green), **C)** pCamkIIα (red), **D)** Oct4, pCamkIIα and Dapi co-staining in mESCs cultured under different conditions (C+L, B2uM, T1nM, C-L, C-L+T1nM) (n=3)

E) Western blot shows the expression of Oct4, Nanog, pSTAT3 and Gapdh in mESCs cultured under different conditions (C+L, B1uM, B2uM, C-L) (n=3).

F) Western blot shows the expression of Oct4, Nanog, pSTAT3 and Gapdh in mESCs cultured under different condition (C+L+T250pM, C+L+T500pM, C+L+T1nM) (n=3)

G) Western blot showed expression of Nanog in mESCs cultured under different conditions (C-L, C-L+T250pM, C-L+T500pM, C-L+T1nM)

H) Western blot showed expression of pSTAT3 and cMyC in mESCs cultured under different conditions (C-L, C-L+T1nM)

I, J) QPCR of pluripotency markers and early differentiation markers under different conditions (C+L, B2uM, T1nM, C-L, C-L+T1nM) (n=5)

K) Brightfield images of the mESCs cultured under different conditions (C+L, B2uM, T1nM, C-L, C-L+T1nM) (n=5)

L) IF detection of Phalloidin in mESCs cultured under different conditions as above (n=3)

M) The bar graph represents the mean intensity of Oct4, Nanog and pCamkII**α** expression calculated from the confocal images of the above experiments (A, B, C).

N) IF detection of E-cadherin staining in mESCs cultured under different conditions (C+L, B2uM, T1nM, C-L)

Note: C+L= Control media + Lif; B1uM= C+L + Bapta 1uM; B2uM = C+ L + Bapta 2uM; T1nM= C+L + thapsigargin 1nM; C-L= control media without Lif; C-L+T1nM = C-L + thapsigargin 1nM; T250 pM, T500pM, and T nM= C+L + thapsigargin (250 pM, 500pM, and 1nM)

The mean intensity was calculated from the confocal images for all experiments using ImageJ software. p-value representation with asterisk <0.05 (*), <0.01 (**), <0.001 (***), <0.0001 (****).

Figure 3: Role of calcium at post-transcriptional level: A) IF detection of dcp1a, β-actin, xrn1a, pCamkIIα, tudor in mESCs cultured under different conditions (C+L, B2uM, T1nM, C-L) (n=3-5) using confocal microscopy at 60x magnification.

B) Co-localization expression profile of dcp1a and β-actin**;** dcp1a and xrn1**;** dcp1a and pCamkIIα**;** dcp1a and tudor in mESCs cultured under different condition (C+L, B2uM, T1nM, C-L, C-L+T1nM). To observe granule size and co-localization of p-bodies and stress

granule markers, the images obtained using a confocal microscope at 60x magnification were cropped to one nucleus size and normalized using a 5uM marker at the bottom.

C) QPCR of p-bodies and stress granule markers (dcp1a, xrn1, **t**udor and pCamkIIα) in the mESCs cultured in the presence of B2uM for 72hrs.

D) The bar graph represents the mean intensity of dcp1a, xrn1, pCamkIIα and **t**udor expression calculated from confocal images from the above experiments (A).

E) IF detection of splicing dependent NMD by using NMD+ GFP, NMD+RFP, NMD-GFP, NMD-RFP reporter in mESCs cultured under different conditions (C+L, B2uM, C-L) (n=3).

F) Splicing-dependent NMD activity was calculated from the confocal images of the above experiments described by Pereverzev et al. 2015.

G) IF detection of long 3' UTR dependent NMD by using SMG+ GFP, SMG+RFP, pTRAM-GFP, pTRAM-RFP reporter in mESCs cultured under different conditions (C+L, B2uM, C-L) (n=3).

H) 3' UTR-dependent NMD activity was calculated from the confocal images of the above experiments as described by Pereverzev et al. 2015.

Note: C+L= Control media + Lif; B2uM = C+ L + Bapta 2uM; T1nM= C+L + thapsigargin 1nM; C-L= control media without Lif; C-L+T1nM = C-L + thapsigargin 1nM

The mean intensity was calculated from the confocal images for all experiments using ImageJ software. p-value representation with asterisk <0.05 (*), <0.01 (**), <0.001 (***), <0.0001 (****).

Figure 4: **Role of calcium at translational level: A)** Polysome profile of C+L and B2uM treated mESCs. (n=5)

B) IF detection of Elf1a expression in mESCs cultured under different conditions (C+L, B2uM, C-L) using confocal microscopy at 60x magnification. (n=3)

C) The bar graph represents the mean intensity of Elf1a expression calculated from the confocal images of the above experiments.

D, E) QPCR of core proliferation and early differentiation markers in the cytoplasmic, 80s, polysome fraction of polysome profiling of control (D2) and B2uM treated mESCs. (n=4)

F, G) QPCR of core proliferation markers and early differentiation markers of mESCS cultured under different conditions (C+L, B2uM, C-**L, C-L+Tti)** for 72hrs followed by combined CHX and ACD treatment (TTi) for 2hr. (n=5)

H) IF detection of brachyury and Nanog expression in mESCs cultured under different conditions (C+L, B2uM, C-L). (n=3)

I) Confocal detection of mitochondria using mitotracker-red staining in mESCs cultured under different conditions (C+L, B2uM, C-L) for 48 hours using confocal microscopy at 40x magnification. To observe the mitochondria shape, images were cropped to one nucleus and normalized using a 5uM marker at the bottom. (n=4)

J) Confocal detection of mitochondria and calcium level using mitotracker-red and fluo-4 co-staining in mESCs cultured under condition (C+L and B2uM) (n=3).

Note: C+L= Control media + Lif; B2uM = C+ L + Bapta 2uM; C-L= control media without Lif; C-L+T1nM = C-L + thapsigargin 1nM

The mean intensity was calculated from the confocal images for all experiments using ImageJ software. p-value representation with asterisk <0.05 (*), <0.01 (**), <0.001 (***), <0.0001 (****).

Figure 5: Role of calcium at post-translational level: IF detection of **A)** Brachyury, and cMyc, **B)** dcp1a, and Tudor, **C)** Oct4 and pUBQ expression mESCs cultured under different

conditions (D2, B2uM and C-L) for 72hrs followed by MG132 (10uM) treatment for 1 hr (n=3).

The bar plot represents the mean intensity of the expression profile of **D)** Brachyury, **E)** cMyc, **F)** dcp1a, and Tudor, **G)** Oct4 and pUBQ from the confocal images of the above experiments.

H) Western blot detection of autophagy marker LC3 in mESCs cultured under different conditions (C+L, B2uM, C-L). (n=3)

I) Cycloheximide chase assay was performed for oct4 and Nanog protein in mESCs cultured under D2, B2uM conditions for 72hrs followed by addition of CHX (50 ug/ml) and chased for every 20min for 1 hr 20 min using western blotting. (n=3)

J) Oct4 and Nanog expression was detected by western blot in mESCs cultured under D2, B2uM conditions for 72hrs followed by the addition of MG132 (10uM) for 1hr. (n=3)

Note: C+L= Control media + Lif; C-L= control media without Lif; D2= C+L+ dmso equivalent to B2uM condition; D2_MG = D2+MG132; B2uM= C+L+ Bapta 2uM; B2_MG = B2uM+MG132; C-L_MG= C-L+MG132

The mean intensity was calculated from the confocal images for all experiments using ImageJ software. p-value representation with asterisk <0.05 (*), <0.01 (**), <0.001 (***), <0.0001 (****).

Figure 6: knockdown of pCamkIIα in mESCsA) Detection of GFP expression of pCamkIIα shRNA and SERCA shRNA transfected by electroporation method in mESCs using fluorescent microscopy at 10X.

Brightfield images showing the morphology of the **B)** control mESCs, **C)** pCamkIIα shRNA (pCamkIIα KD) and SERCA shRNA (SER_R2_KD) transfected mESCs at 48hrs.

D) QPCR of pCamkIIα and serca R2 receptor expression in the mESCs at 48hrs upon pCamkIIα KD and SER_R2_ KD respectively

E) QPCR of pCamkIIα expression in the SER_R2 KD mESCs and serca_R2 receptor expression in the pCamkIIα KD mESCs at 48hrs.

F, G) Western blot detection of Oct4, Nanog, pSTAT3, and Gapdh expression in the pCamkIIα KD and SER_R2_KD mESCs at 48hrs (n=3)

H, I) IF detection of DCP1a and pCamkIIα co-expression in pCamkIIα and SER_R2 KD mESCs at 48hrs. (n=3)

J, K) Bar plot represents the mean intensity of pCamkIIα and dcp1a expression in mESCs calculated from the confocal images of the above experiments

L) QPCR of p-bodies and stress granule markers in the mESCs at 48hrs upon pCamkIIα KD and ser_R2 KD. (n=4)

M, N) QPCR of pluripotency and differentiation markers in the mESCs at 48hrs upon pCamkIIα KD and SER_R2 KD. (n=3)

Note: The mean intensity was calculated from the confocal images for all experiments using ImageJ software. p-value representation with asterisk <0.05 (*), <0.01 (**), <0.001 (***), <0.0001 (****).

Figure 7: Calcium and phosphoproteomics in mESCs: A) Heat map shows log2fold change of DEPP in B2uM treated mESCs compared to D2 (control) mESCs detected by mass spectrometry (n=2)

B, C, E) KEGG pathway and GOC enrichment analysis was done using ShinyGO 0.80 software for the DEPP represented in the heat map (A).

D) The hierarchical clustering tree shows the correlation among the most significant pathways found in KEGG pathway enrichment analysis for all DEPP.

F) The bar plot shows the string enrichment function analysis of all the DEPP demonstrated in the heat map.

G, H) KEGG pathway enrichment analysis was done for spliceosome and mRNA surveillance pathways all the DEPP represented in heat map (A).

I) String PPI network analysis was performed for all DEPP represented in a heat map (A).

Note: Arrow represent the upregulated and downregulated genes

Note: C+L= Control media + Lif; B2uM = C+ L + Bapta 2uM; D2= C+L+ dmso equivalent to B2uM condition

p-value representation with asterisk <0.05 (*), <0.01 (**), <0.001 (***), <0.0001 (****).

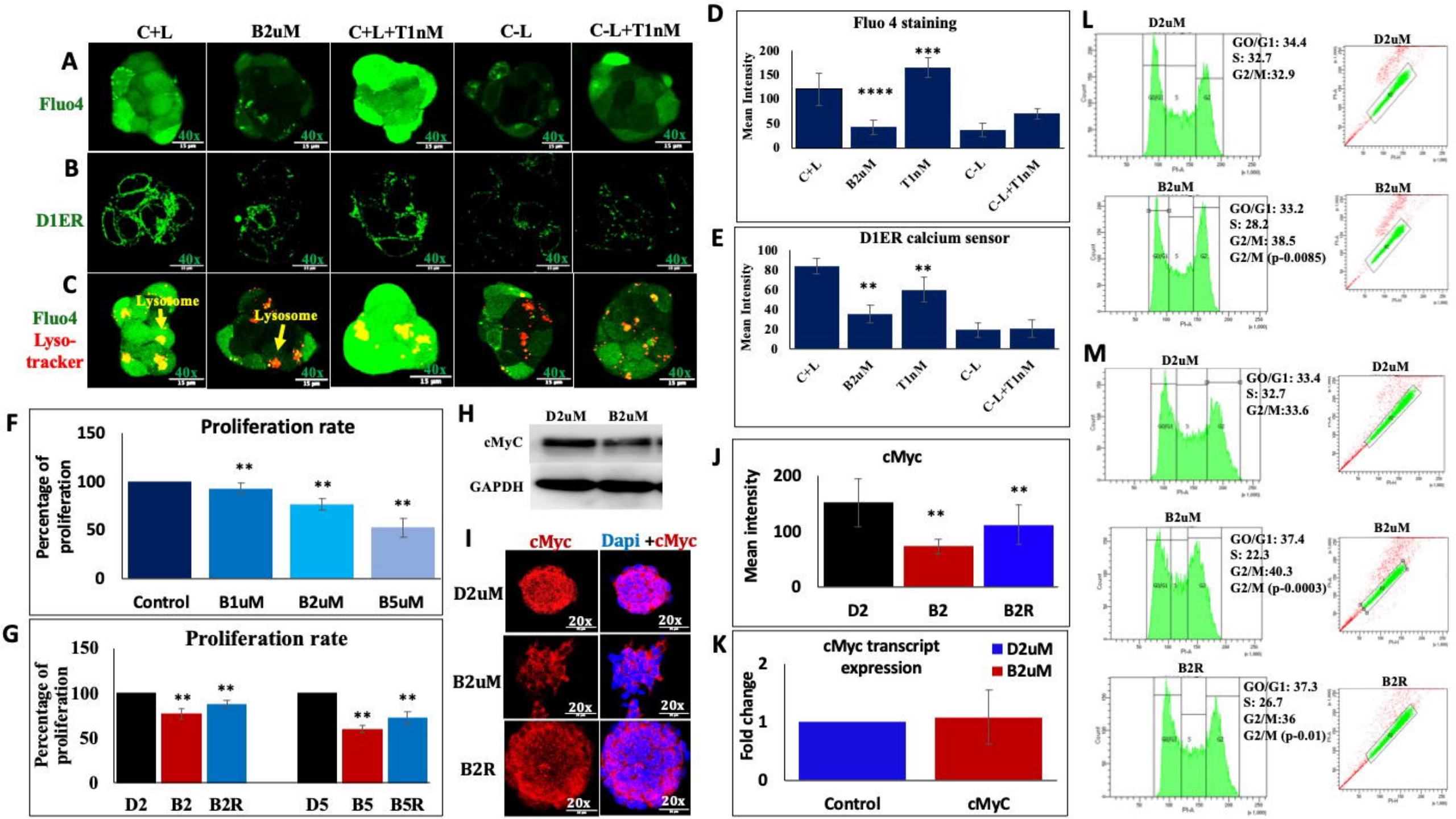
C+L
B2uM
C+L+T1nM
C-L
C-L+T1nM
A
Fluo4
B
D1ER
C
Fluo4
Lyso-tracker
Lysosome
Lysosome
40x
D
Fluo 4 staining
Mean Intensity
200
150
100
50
0
****
***
C+L
B2uM
T1nM
C-L
C-L+T1nM
E
D1ER calcium sensor
Mean Intensity
100
80
60
40
20
0
**
**
C+L
B2uM
T1nM
C-L
C-L+T1nM
F
Proliferation rate
Percentage of proliferation
150
100
50
0
**
**
**
Control
B1uM
B2uM
B5uM
G
Proliferation rate
Percentage of proliferation
150
100
50
0
**
**
**
**
D2
B2
B2R
D5
B5
B5R
H
D2uM
B2uM
cMyC
GAPDH
I
cMyc
Dapi +cMyc
D2uM
B2uM
B2R
20x
J
cMyc
Mean intensity
200
100
0
**
**
D2
B2
B2R
K
cMyc transcript expression
D2uM
B2uM
Fold change
2
1
0
Control
cMyC
L
D2uM
GO/G1: 34.4
S: 32.7
G2/M:32.9
B2uM
GO/G1: 33.2
S: 28.2
G2/M: 38.5
G2/M (p-0.0085)
M
D2uM
GO/G1: 33.4
S: 32.7
G2/M:33.6
B2uM
GO/G1: 37.4
S: 22.3
G2/M:40.3
G2/M (p-0.0003)
B2R
GO/G1: 37.3
S: 26.7
G2/M:36
G2/M (p-0.01)

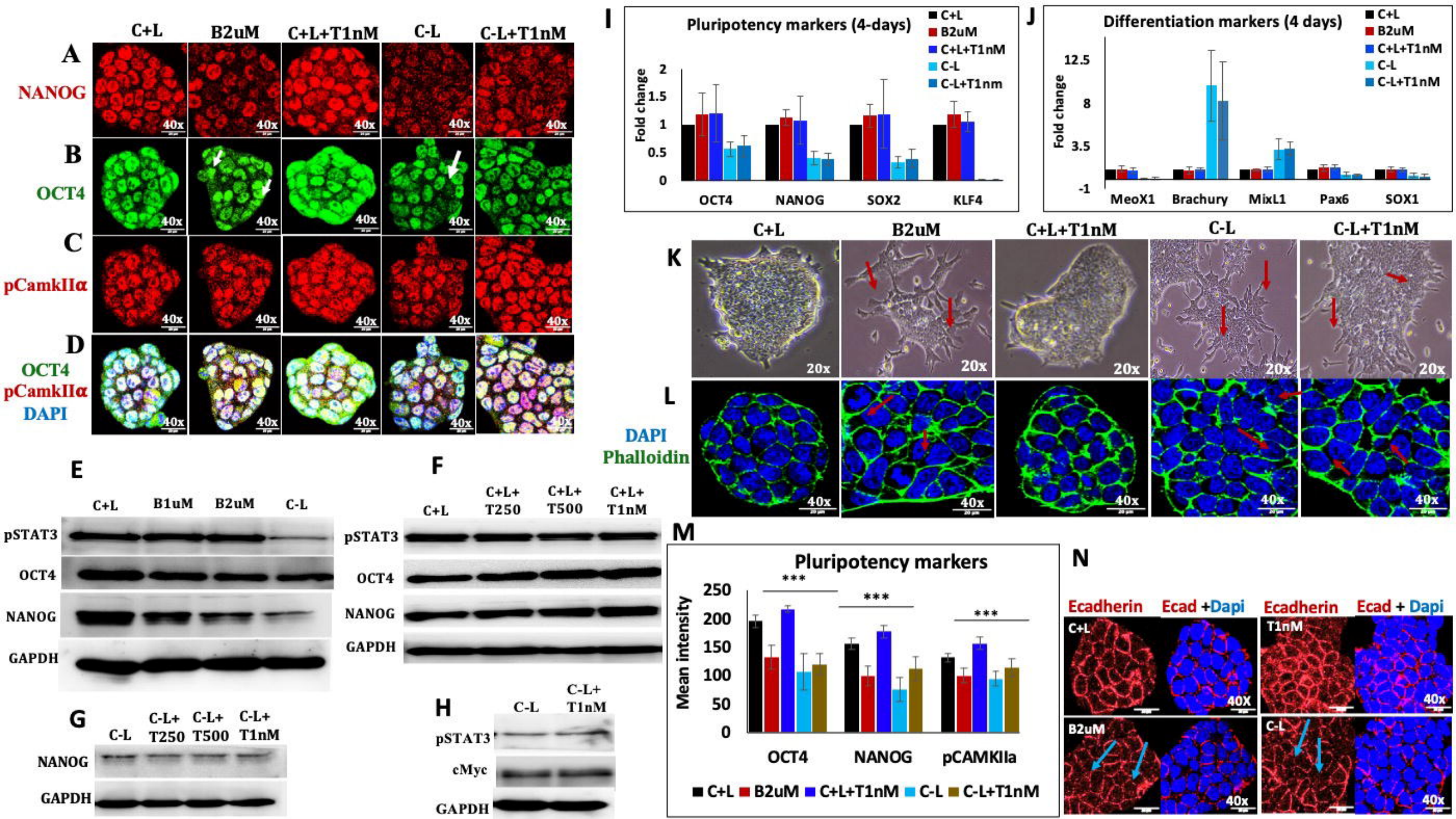
A
NANOG
B
OCT4
C
pCamkIIα
D
OCT4
pCamkIIα
DAPI
C+L
B2uM
C+L+T1nM
C-L
C-L+T1nM
40x
E
C+L
B1uM
B2uM
C-L
pSTAT3
OCT4
NANOG
GAPDH
F
C+L
C+L+ T250
C+L+ T500
C+L+ T1nM
pSTAT3
OCT4
NANOG
GAPDH
G
C-L
C-L+ T250
C-L+ T500
C-L+ T1nM
NANOG
GAPDH
H
C-L
C-L+ T1nM
pSTAT3
cMyc
GAPDH
I
Pluripotency markers (4-days)
Fold change
OCT4
NANOG
SOX2
KLF4
C+L
B2uM
C+L+T1nM
C-L
C-L+T1nm
J
Differentiation markers (4 days)
Fold change
MeoX1
Brachury
MixL1
Pax6
SOX1
K
20x
L
DAPI
Phalloidin
40x
M
Pluripotency markers
Mean intensity
OCT4
NANOG
pCAMKIIa
***
N
Ecadherin
Ecad +Dapi
Ecadherin
Ecad + Dapi
C+L
T1nM
B2uM
C-L
40X

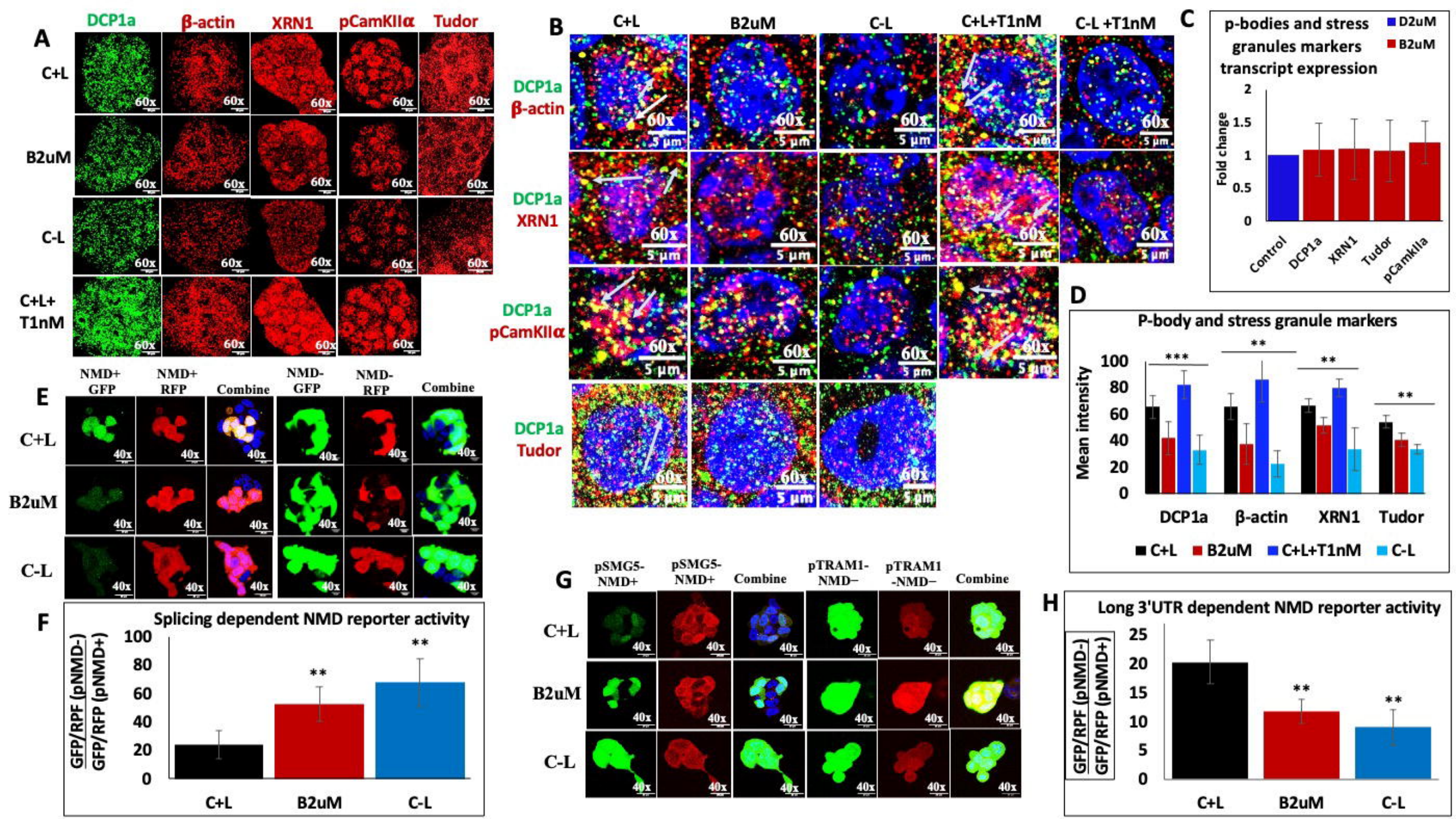
A
DCP1a
β-actin
XRN1
pCamKIIα
Tudor
C+L
B2uM
C-L
C+L+ T1nM
60x
B
C+L
B2uM
C-L
C+L+T1nM
C-L +T1nM
DCP1a β-actin
DCP1a XRN1
DCP1a pCamKIIα
DCP1a Tudor
5 µm
C
p-bodies and stress granules markers transcript expression
D2uM
B2uM
Fold change
Control
DCP1a
XRN1
Tudor
pCamkIIa
D
P-body and stress granule markers
Mean intensity
DCP1a
β-actin
XRN1
Tudor
C+L
B2uM
C+L+T1nM
C-L
E
NMD+ GFP
NMD+ RFP
Combine
NMD- GFP
NMD- RFP
Combine
C+L
B2uM
C-L
40x
F
Splicing dependent NMD reporter activity
GFP/RPF (pNMD-)
GFP/RFP (pNMD+)
C+L
B2uM
C-L
G
pSMG5-NMD+
pSMG5-NMD+
Combine
pTRAM1-NMD−
pTRAM1 -NMD−
Combine
C+L
B2uM
C-L
H
Long 3'UTR dependent NMD reporter activity
GFP/RPF (pNMD-)
GFP/RFP (pNMD+)
C+L
B2uM
C-L

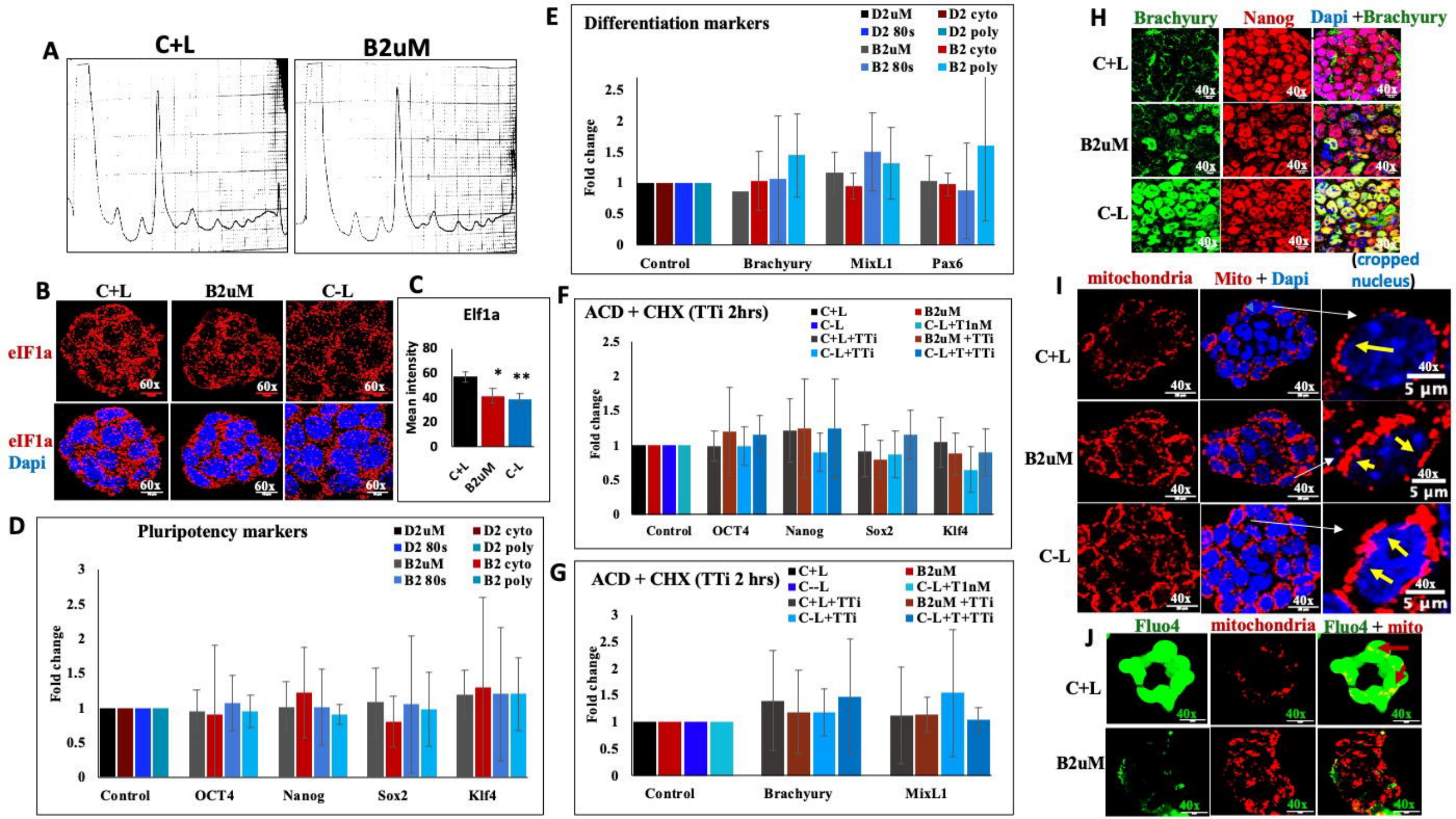
A
C+L
B2uM
B
C+L
B2uM
C-L
eIF1a
eIF1a
Dapi
60x
C
Elf1a
Mean intensity
80
60
40
20
0
*
**
C+L
B2uM
C-L
D
Pluripotency markers
D2uM
D2 cyto
D2 80s
D2 poly
B2uM
B2 cyto
B2 80s
B2 poly
Fold change
3
2.5
2
1.5
1
0.5
0
Control
OCT4
Nanog
Sox2
Klf4
E
Differentiation markers
D2uM
D2 cyto
D2 80s
D2 poly
B2uM
B2 cyto
B2 80s
B2 poly
Fold change
2.5
2
1.5
1
0.5
0
Control
Brachyury
MixL1
Pax6
F
ACD + CHX (TTi 2hrs)
C+L
B2uM
C-L
C-L+T1nM
C+L+TTi
B2uM +TTi
C-L+TTi
C-L+T+TTi
Fold change
2.5
2
1.5
1
0.5
0
Control
OCT4
Nanog
Sox2
Klf4
G
ACD + CHX (TTi 2 hrs)
C+L
B2uM
C--L
C-L+T1nM
C+L+TTi
B2uM +TTi
C-L+TTi
C-L+T+TTi
Fold change
3
2.5
2
1.5
1
0.5
0
Control
Brachyury
MixL1
H
Brachyury
Nanog
Dapi +Brachyury
C+L
B2uM
C-L
40x
I
mitochondria
Mito + Dapi
(cropped nucleus)
C+L
B2uM
C-L
40x
5 µm
J
Fluo4
mitochondria
Fluo4 + mito
C+L
B2uM
40x

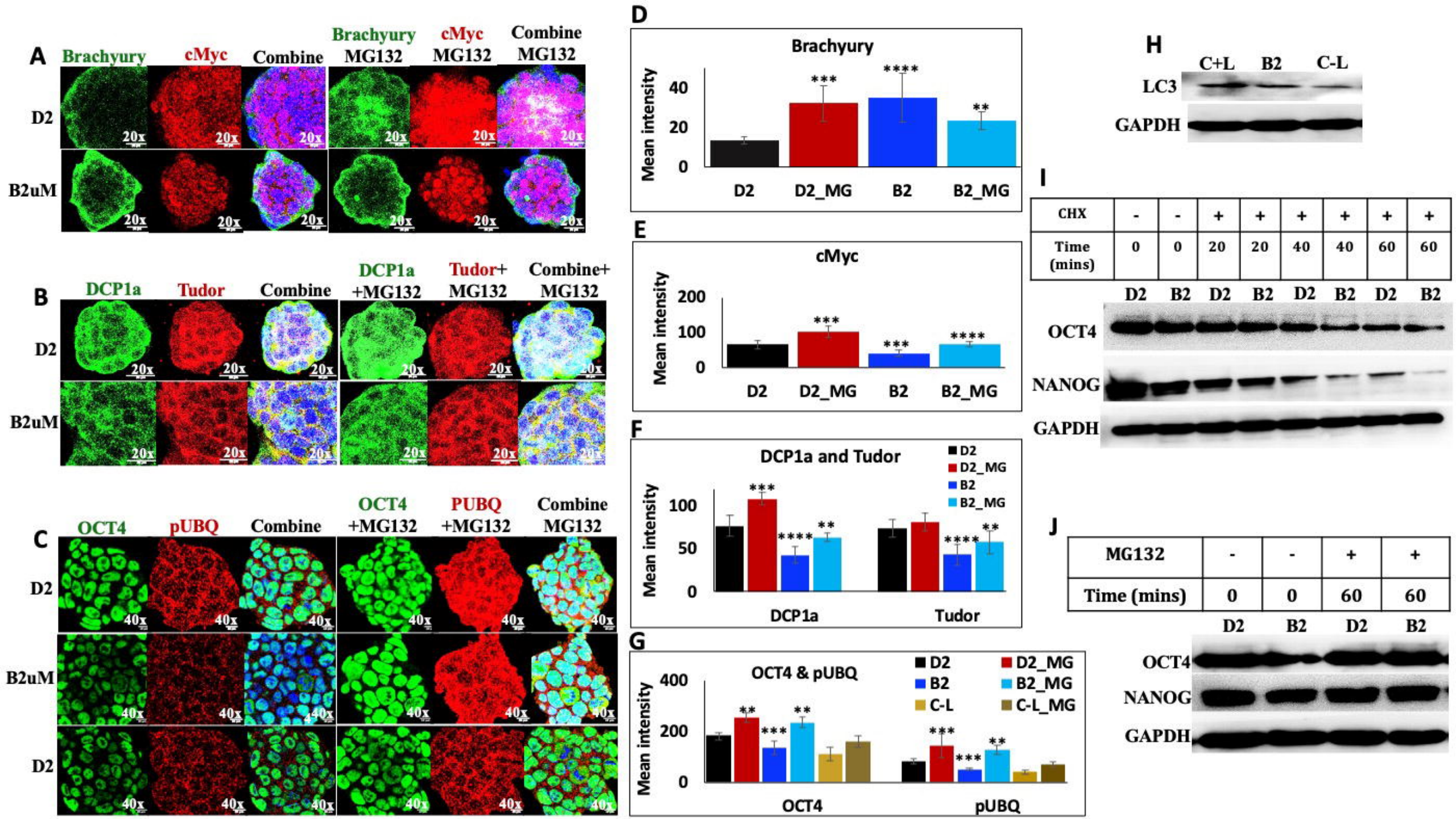
A
Brachyury
cMyc
Combine
Brachyury MG132
cMyc MG132
Combine MG132
D2
B2uM
20x
B
DCP1a
Tudor
Combine
DCP1a +MG132
Tudor+ MG132
Combine+ MG132
C
OCT4
pUBQ
Combine
OCT4 +MG132
PUBQ +MG132
Combine MG132
40x
D
Brachyury
Mean intensity
D2
D2_MG
B2
B2_MG
E
cMyc
F
DCP1a and Tudor
DCP1a
Tudor
G
OCT4 & pUBQ
OCT4
pUBQ
C-L
C-L_MG
H
C+L
LC3
GAPDH
I
CHX
Time (mins)
OCT4
NANOG
J
MG132

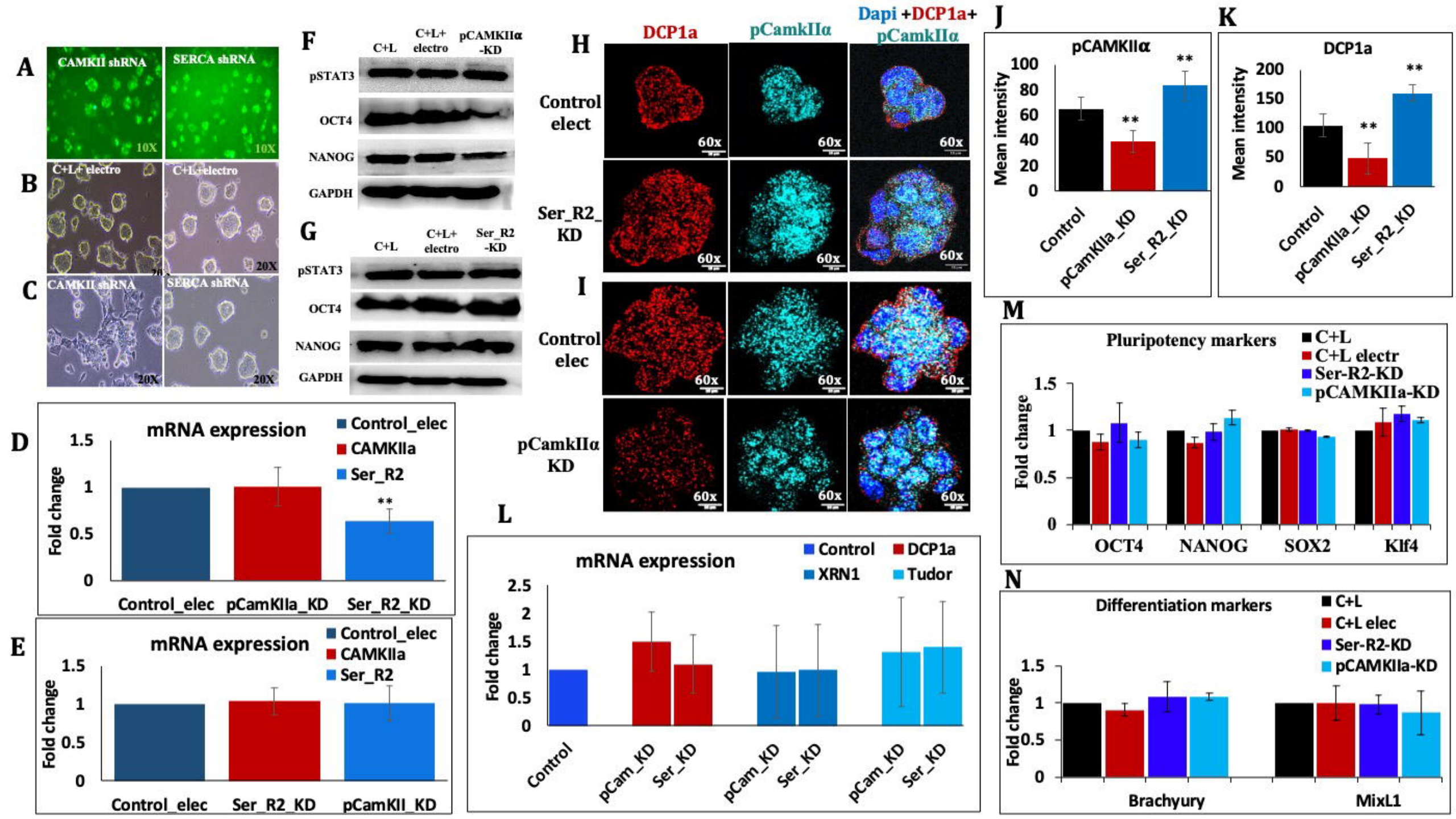
A
CAMKII shRNA
SERCA shRNA
10X
10X
B
C+L+ electro
C+L+electro
20X
20X
C
CAMKII shRNA
SERCA shRNA
20X
20X
F
C+L
C+L+ electro
pCAMKIIα -KD
pSTAT3
OCT4
NANOG
GAPDH
G
C+L
C+L+ electro
Ser_R2 -KD
pSTAT3
OCT4
NANOG
GAPDH
H
DCP1a
pCamkIIα
Dapi +DCP1a+ pCamkIIα
Control elect
Ser_R2_ KD
60x
I
Control elec
pCamkIIα KD
60x
J
pCAMKIIα
Mean intensity
100
80
60
40
20
0
**
**
Control
pCamKIIa_KD
Ser_R2_KD
K
DCP1a
Mean intensity
200
150
100
50
0
**
**
Control
pCamKIIa_KD
Ser_R2_KD
M
Pluripotency markers
C+L
C+L electr
Ser-R2-KD
pCAMKIIa-KD
Fold change
1.5
1
0.5
0
OCT4
NANOG
SOX2
Klf4
D
mRNA expression
Control_elec
CAMKIIa
Ser_R2
Fold change
1.5
1
0.5
0
**
Control_elec
pCamKIIa_KD
Ser_R2_KD
E
mRNA expression
Control_elec
CAMKIIa
Ser_R2
Fold change
1.5
1
0.5
0
Control_elec
Ser_R2_KD
pCamKII_KD
L
mRNA expression
Control
DCP1a
XRN1
Tudor
Fold change
2.5
2
1.5
1
0.5
0
Control
pCam_KD
Ser_KD
pCam_KD
Ser_KD
pCam_KD
Ser_KD
N
Differentiation markers
C+L
C+L elec
Ser-R2-KD
pCAMKIIa-KD
Fold change
1.5
1
0.5
0
Brachyury
MixL1

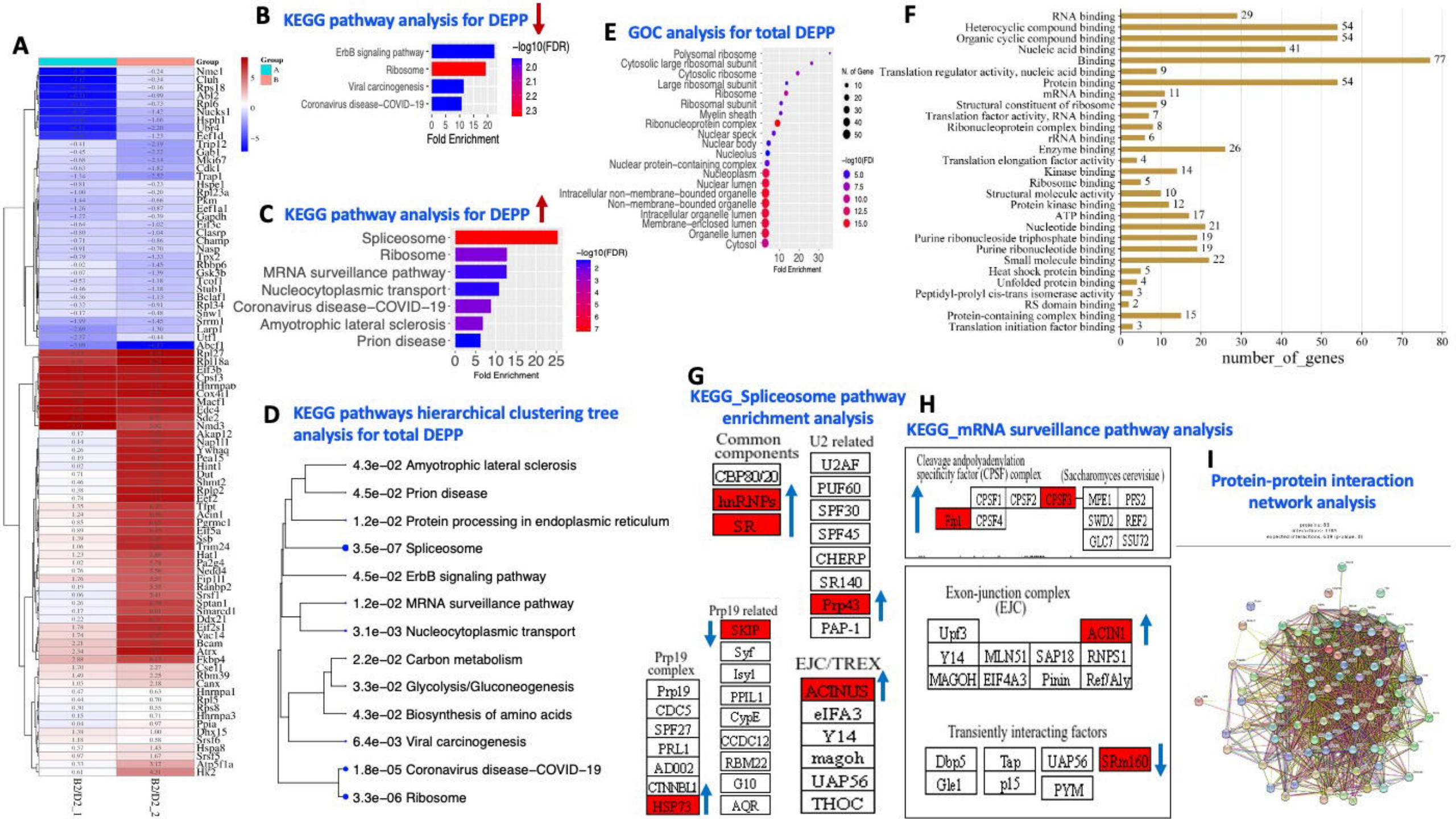
A
Group
Nmc1
Cluh
Rps18
Abl2
Rpl6
Nucks1
Hsph1
Ubr4
Eef1d
Trip12
Gab1
Mki67
Cdk1
Trap1
Hspe1
Rpl23a
Pkm
Eef1a1
Gapdh
Eif3c
Clasrp
Champ
Nasp
Tpx2
Rbbp6
Gsk3b
Tcof1
Stub1
Bclaf1
Rpl34
Snw1
Srrm1
Larp1
Utf1
Abcf1
Rpl27
Rpl18a
Eif3b
Cpsf3
Hnrnpab
Cox4i1
Macf1
Edc4
Sde2
Nmd3
Akap12
Nap1l1
Ywhaq
Pea15
Hint1
Dut
Shmt2
Rplp2
Eef2
Tipt
Acin1
Pgrmc1
Eif5a
Ssb
Trim24
Hat1
Pa2g4
Nedd4
Fip1l1
Ranbp2
Srsf1
Sptan1
Smarcd1
Ddx21
Eif2s1
Vac14
Bcam
Atrx
Fkbp4
Cse1l
Rbm39
Canx
Hnrnpa1
Rpl5
Rps8
Hnrnpa3
Ppia
Dhx15
Srsf6
Hspa8
Srsf5
Atp5f1a
HK2
B2/D2_1
B2/D2_2
B
KEGG pathway analysis for DEPP
ErbB signaling pathway
Ribosome
Viral carcinogenesis
Coronavirus disease-COVID-19
Fold Enrichment
-log10(FDR)
C
KEGG pathway analysis for DEPP
Spliceosome
Ribosome
MRNA surveillance pathway
Nucleocytoplasmic transport
Coronavirus disease-COVID-19
Amyotrophic lateral sclerosis
Prion disease
Fold Enrichment
-log10(FDR)
D
KEGG pathways hierarchical clustering tree analysis for total DEPP
4.3e-02 Amyotrophic lateral sclerosis
4.5e-02 Prion disease
1.2e-02 Protein processing in endoplasmic reticulum
3.5e-07 Spliceosome
4.5e-02 ErbB signaling pathway
1.2e-02 MRNA surveillance pathway
3.1e-03 Nucleocytoplasmic transport
2.2e-02 Carbon metabolism
3.3e-02 Glycolysis/Gluconeogenesis
4.3e-02 Biosynthesis of amino acids
6.4e-03 Viral carcinogenesis
1.8e-05 Coronavirus disease-COVID-19
3.3e-06 Ribosome
E
GOC analysis for total DEPP
Polysomal ribosome
Cytosolic large ribosomal subunit
Cytosolic ribosome
Large ribosomal subunit
Ribosome
Ribosomal subunit
Myelin sheath
Ribonucleoprotein complex
Nuclear speck
Nuclear body
Nucleolus
Nuclear protein-containing complex
Nucleoplasm
Nuclear lumen
Intracellular non-membrane-bounded organelle
Non-membrane-bounded organelle
Intracellular organelle lumen
Membrane-enclosed lumen
Organelle lumen
Cytosol
Fold Enrichment
N. of Gene
-log10(FDR)
F
RNA binding
Heterocyclic compound binding
Organic cyclic compound binding
Nucleic acid binding
Binding
Translation regulator activity, nucleic acid binding
Protein binding
mRNA binding
Structural constituent of ribosome
Translation factor activity, RNA binding
Ribonucleoprotein complex binding
rRNA binding
Enzyme binding
Translation elongation factor activity
Kinase binding
Ribosome binding
Structural molecule activity
Protein kinase binding
ATP binding
Nucleotide binding
Purine ribonucleoside triphosphate binding
Purine ribonucleotide binding
Small molecule binding
Heat shock protein binding
Unfolded protein binding
Peptidyl-prolyl cis-trans isomerase activity
RS domain binding
Protein-containing complex binding
Translation initiation factor binding
number_of_genes
G
KEGG_Spliceosome pathway enrichment analysis
Common components
CBP80/20
hnRNPs
SR
U2 related
U2AF
PUF60
SPF30
SPF45
CHERP
SR140
Prp43
PAP-1
Prp19 related
SKIP
Syf
Isy1
PPIL1
CypE
CCDC12
RBM22
G10
AQR
Prp19 complex
Prp19
CDC5
SPF27
PRL1
AD002
CTNNBL1
HSP73
EJC/TREX
ACINUS
eIFA3
Y14
magoh
UAP56
THOC
H
KEGG_mRNA surveillance pathway analysis
Cleavage andpolyadenylation specificity factor (CPSF) complex
(Saccharomyces cerevisiae)
CPSF1
CPSF2
CPSF3
Fip1
CPSF4
MPE1
PFS2
SWD2
REF2
GLC7
SSU72
Exon-junction complex (EJC)
Upf3
ACIN1
Y14
MLN51
SAP18
RNPS1
MAGOH
EIF4A3
Pinin
Ref/Aly
Transiently interacting factors
Dbp5
Tap
UAP56
SRm160
Gle1
p15
PYM
I
Protein-protein interaction network analysis